PROJECTION OF FUTURE STREAM FLOW AND THEIR UNCERTAINTY OVER WEST RAPTI BASIN, NEPAL

NITESH SHRESTHA

APRIL, 2017

SUPERVISORS:

Dr. Ing. T.H.M. Rientjes

Dr. Y. Zeng

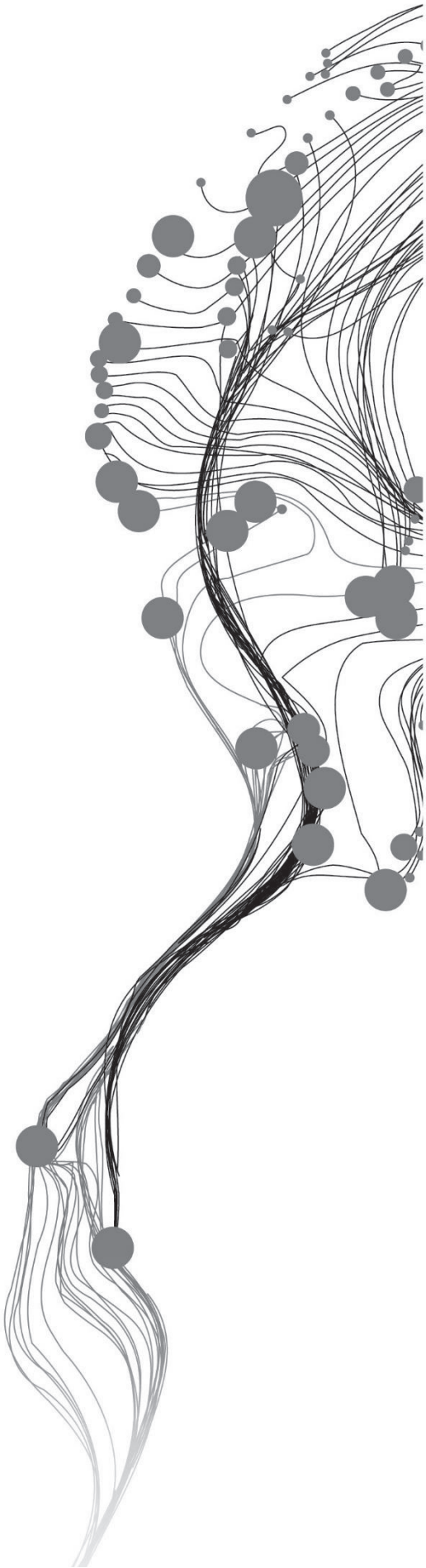

PROJECTION OF FUTURE STREAMFLOW AND THEIR UNCERTAINTY OVER WEST RAPTI BASIN, NEPAL

NITESH SHRESTHA

Enschede, The Netherlands, April, 2017

Thesis submitted to the Faculty of Geo-Information Science and Earth Observation of the University of Twente in partial fulfilment of the requirements for the degree of Master of Science in Geo-information Science and Earth Observation.
Specialization: Water Resources and Environmental Management

SUPERVISORS:
Dr. Ing. T.H.M. Rientjes
Dr. Y. Zeng

THESIS ASSESSMENT BOARD:
Dr. Ir. C. van der Tol (Chair)]
Dr. Ir. Martijn J. Booij (External Examiner, University of Twente)

ABSTRACT

Analysis of regional climate simulation to evaluate the ability of Coordinated Regional Climate Downscaling Experiment in South Asia (CORDEX-South Asia) to simulate climate variability and extremes, and capture temperature and precipitation climatology over Nepal is analysed. The analysis of regional climate models (RCMs) combine three-step sequential climate model selection procedure which involved selection of climate models for two representative concentration pathways (RCP) 4.5 and 8.5 based on (i) range of projected changes in climatic means, (ii) range of projected change in climatic extremes, and (iii) climate model skill to simulate past climate. Climatology of the study area have been assessed against the gridded observational dataset: Asian Precipitation-Highly Resolved Observational Data Integration Towards the Evaluation of Water Resources (APHRODITE). Changes in climate are analysed between 1976-2005 and 2071-2100 for RCP 4.5 and RCP 8.5. Thus finalized RCMs are further bias-corrected through empirical quantile mapping technique. Moreover, HBV Light model is set up for West Rapti Basin in Nepal, and future flows are simulated with- and without-bias corrected RCMs. Finally, extreme low flow and high flows have been analysed based on frequency distribution of daily stream flows.

Results show that the RCMs show a wide variation among themselves and individually over time in simulating temperature and precipitation distribution over the study region. It indicates the inability of RCMs to simulate regional climate, and uncertainty in climate projections. Results on comparison of historical simulations by RCMs with APHRODITE for 1976-2005 show under-estimation of mean annual temperature cycle which range from 0.2 ^{0}C to 7.6 ^{0}C. However, precipitation is over-estimated by all models, except for ICHEC-EC-EARTH. Bias-corrected RCM simulations indicate towards rise of annual average temperature by 1.4 – 2.3 ^{0}C for RCP 4.5, and by 3 – 3.9 ^{0}C for RCP 8.5 by the end of the century. Similarly, annual average precipitation is likely to increase by 109 mm to 414 mm for RCP 4.5, and by 337 mm to 488 mm for RCP 8.5 in future period.

Temporal shift of peak runoff generation is observed from August to July, based on bias-corrected projections for both RCPs. Overall decrease in mean monthly stream flows has been observed during monsoon while there is increase in low flows. However, frequency distribution of high flows indicate towards marked increase for discharge values greater than 990 cubic meter per second, while occurrence of low flows also shows increment in future.

Keywords: CORDEX South Asia, RCM, RCP, bias correction, HBV Light model

ACKNOWLEDGEMENTS

Thank you, Pravu Jee

It is my biggest pleasure to be guided by Dr. Ing. Tom Rientjes, as my first supervisor. I am grateful that I got an opportunity to receive regular suggestions and comments from him, and this document is the result of his incessant support, efforts and attention to my works. I just wish if we had more time to discuss on hydrological modelling. I would also like to thank Dr. Y. Zeng as my second supervisor for his support.

I would like to extend my gratitude to Dr. A.F. Lutz for his prompt response to my queries through email, and also Dr. Ir. HW ter Maat for his guidance through personal visit, and helping me. It was beyond my imagination, and thank you Dr. Maat.

I am grateful to M.C.F. Metz-Bekkers, T.B. van den Boogaard, Dr. Ir. S. Salama and Ir. A.M. van Lieshout for their valuable support during my hard times. Thank you Arno for your precious support.

Dear Pravu Jee, thank you very much for guiding me all my life, and supporting me in pursuing my dreams every time. You are the true, and only inspiration to my life. I wish I could show you now, the skills I have learnt.

Dear Maau, thank you so much for allowing me to get here, and loving me all the times. I just wish Pravu Jee is still with us to share the happiness on the skills I have learnt so far.

Dear Mumun, my beautiful wife, thank you my love. I know that it is hard to live a single moment without sharing our stories together, but you took that pain for my goodness. I am very grateful to you.

Thank you to all my family members for your continuous support, love and care.

My sincere gratitude goes to the friends, faculty and staff at ITC along with my beautiful friends from ITC restaurant.

Contents

List of Figures

List of Tables

1. INTRODUCTION

This chapter provides an introduction to the research. Background and relevance to the research is discussed in section 1.1 along with past relevant researches. Problem statement and existing research gaps are discussed in section 1.2 and section 1.3 respectively. Research objective, research questions and hypothesis for this research are presented in section 1.4, section 1.5 and section 1.6 respectively.

1.1. Background and Relevance

Water is indispensable for all forms of life (Bates, Kundzewicz, Wu, & Palutikof, 2008). Water resources is a boon to survival and development of the society, yet nuisance at times. Availability and sustainable management of water resources defines social and economic development (Gohar & Cashman, 2016), yet extreme meteorological and hydrological events all may lead to major disasters and result in heavy social and economic losses, and even severe health consequences (Basin, Tian, Zhao, Li, & Tian, 2011). Global fresh water system is under immense pressure due to anthropogenic activities, mainly global change and climate change.

Climate change has further exacerbated the impact on water resources regarding its availability and distribution spatially and temporally (Bae, Jung, & Lettenmaier, 2011). Despite the levels of uncertainty associated with the magnitude and direction of climate variability and change, it is unequivocal – "observational records and climate projections provide abundant evidence that freshwater resources are vulnerable and have the potential to be strongly impacted by climate change, with wide-ranging consequences for human societies and ecosystems" (Bates et al., 2008). It is very likely to alter the quality and quantity of water reserves globally in terms of availability, distribution, agricultural activities, and human and ecosystem functions. Other effects include magnitude and timing of runoff, frequency and intensity of floods and droughts, rainfall patterns, and extreme weather events (Jiang et al., 2007). Distinguishing characteristics of studies carried out to assess impact of climate change on water resources is tabulated in Table 1.

The common practice for assessing the impacts of climate change on water resources is to first project future climate provided by general circulation models (GCMs). The spatial resolution of GCMs is too coarse (~250 km) to represent regional climate variations, and topographic processes at the scales (20-50 km) required for water resources impact assessment (Wilby et al., 2000); (Minville & Leconte, 2008). Thus outputs from GCMs are downscaled from global to regional scale using empirical-statistical downscaling methods or for simulating sub-GCM grid scale climate features dynamically for regional climate models (RCMs) simulations. Statistical methods are more straightforward than dynamical downscaling but tend to underestimate variance and poorly represent extreme events because of partly relationship between regional and local climate variability, and large scale climate variations, and thus statistical techniques like regression methods tend to under-predict climatic variability (Fowler, Blenkinsop, & Tebaldi, 2007). In regions with complex topography, the dynamical downscaling of

GCM simulations has a unique importance in addressing precipitation due to orography as it incorporates model physics rather than statistical relationship. However, studies have showed that existing approaches have difficulty in downscaling in mountainous terrain (Samuelsson et al., 2011). Finally, the outputs of downscaling is further used to assess future climatic changes, and run hydrological models for climate change impact studies.

Selection of climate models are often based on simply averaging all model simulated climate variables with available data, generally examining only the mean climate. This particularly results into equal weighting to all the models as models that poorly simulates the area of interest are equally weighted with those that closely simulates compared to observation data. Another approach uses metrics of model skill to prequalify models based on their ability to simulate climatological variables of interest from the entire pool of available models (Pierce, Barnett, Santer, & Gleckler, 2009).

Researchers developed hydrological models to describe dynamic and non-linear transformation of precipitation into streamflow via processes such as surface, sub-surface and groundwater flows, infiltration, interception, evaporation, transpiration, snowmelt, etc. Purpose of the study and model availability largely determines the choice of a model (Xu, 1999). Arnell, 1992 and Gleick, 1986 found that monthly water balance models are useful in assessing water resource management in a regional scale to identify the hydrologic consequences of changes in temperature, precipitation and other climatic variables. Conceptual lumped-parameter models are widely used for detailed assessments of surface flow, and also has been used by many researchers to assess the impact of climate change (Bastola, Murphy, & Sweeney, 2011). Similarly, process based distributed parameter models are needed to simulate spatial patterns of hydrologic response (Kour, Patel, & Krishna, 2016).

Table 1 Distinguishing characteristics of studies carried out to assess impact of climate change on water resources

Author(s)	Study basin	Climate model/s (Scenario)	Downscaling Method (if any)	Baseline period	Future climate change projection	Hydrological model(s)	Results
(Abdo, Fiseha, Rientjes, Gieske, & Haile, 2009)	Gilgel Abbay Catchment, Ethiopia	HadCM3; A2 and B2	SDSM	1961-1990	2011-2040 2041-2070 2071-2099	HBV	• In the main rainy season (June-September) the runoff volume will reduce by 11.6% and 10.1% for A2 and B2 scenario respectively in 2080s. • The mean annual runoff will reduce by 2.6% and 2.9% for A2 and B2 scenario respectively within the same period
(Bae et al., 2011)	Chungju Dam Basin, Korea	13 GCMs; A2, A1B, B1	WXGEN	1971-2000	2011-2040 2071-2100	PRMS, SWAT, SLURP	• Relative seasonal runoff changes are dominantly affected by GCMs rather than hydrological models • However, winter runoff changes are also sensitive to different hydrological models. • PET computation methods affect runoff changes, although the magnitudes of the differences vary among the hydrological models
(Baguis, Roulin, Willems, & Ntegeka, 2010)	Gete and Ourthe	PRUDENCE 11 RCMs; A2, B2	Bias correction: Delta Method	1961-1990	2071-2100	SCHEME	• Low flow events will undergo a very strong amplification under climate change • Average of high flow over the ensemble of the scenario simulations differs only by little from the control value

(Biemans et al., 2013)	Indus, Ganges, Brahmaputra, Godavari, Krishna; India	HadRM3, REMO; A1B		1971-2000	2036-2065	LPjml	
(Dams, Nossent, Senbeta, Willems, & Batelaan, 2015)	Kleine Nete Catchment, Belgium	All RCMs from PRUDENCE and IPCC AR4 database		1961-1990	2071-2100	WetSpa, SWAT, PRMS	• Uncertainty due to the hydrological model structure becomes higher than the uncertainty due to the climate change scenarios
(Gu et al., 2014)	Yangtze river basin	RegCM4.0, A1B	Distribution Mapping ; Linear Scaling	1970-1999	2070-2099	VIC	• For the maximum daily dis- charge and maximum 7 days water volume, the original extreme flood with return periods of 50, 20, and 10 years will change into floods with return periods of approximately 15, 7, and 3 years. • For the maximum 15 days water volume, the original extreme flood with return periods of 50, 20, and 10 years will change into floods with the return period of approximately 10, 5, and 3 years.

1.2. Problem Statement

A large number of climate models are available today and indicates the need to inter-compare model performance such as shown in Coupled Model Inter-comparison Project Phase 3 (CMIP3) in 2007 (25 different GCMs) whereas CMIP5 archive in 2013 contains around 61 different GCMs. However, detailed climate change impact studies cannot include all these projections (Lutz et al., 2016). The general approach is to select one climate model or small ensemble of climate models for assessment while the selection of these models itself is not straightforward and depends on multiple criteria.

Ghimire, Choudhary, & Dimri, 2015 assessed the performance of 11 CORDEX South Asia experiments to evaluate their ability in capturing and characterizing the precipitation climatology, and concluded that the experiments showed wide variation in capturing precipitation over time and space. Although RCMs are increasingly being used for hydrological studies as they transfer large-scale information from GCMs (~250 km) to RCM scales (20-50 km) which are closer to catchment scale, RCMs simulated hydrological components do not often agree with streamflow observations. RCM simulated climate variables such as temperature and precipitation also show significant biases (Teutschbein & Seibert, 2010) possibly due to imperfect conceptualization, discretization and spatial averaging with grid cells.

The climate projection uncertainties and downscaling uncertainties have been extensively explored, however little attention is given on the uncertainties stemming from hydrologic model parameters and structures. Equifinality of model parameter sets, quality and quantity of available observation data used for parameter estimation, and the choice of model calibration period leads to uncertainties of hydrological model parameters (Bae et al., 2011). Jiang et al., 2007 compared the hydrological impact of climate change using six hydrological models in Dongjian basin, South China and came out with large differences in model predicted runoff using the same alternative climates as input to the models.

Hingray, Mezghani, and Buishand (2008) concluded that the uncertainty resulting from climate model is larger than uncertainty associated with hydrological model, and contributes the largest part to the total impact-prediction uncertainty for mean and low hydrological impact-climate change scenario. Similarly Minville & Leconte, 2008 also concluded that the largest uncertainty comes from the choice of GCM in assessing impact of climate change on hydrology. Finger, Heinrich, Gobiet, & Bauder, 2012 had also similar remarks that largest fraction of uncertainty was propagated to the end-result by climate model uncertainty. Other studies show that hydrological model structure introduces a large uncertainty on both average monthly discharge and the extremes peak and low flow predictions under high impact climate change scenarios (Bastola, Murphy, & Sweeney, 2011; Bae et al., 2011; Dams, Nossent, Senbeta, Willems, & Batelaan, 2015).

1.3. Research Gap

Lutz et al., 2016 presented three step sequential GCM selection procedure for major river basins of South Asia. Rajbhandari, Shrestha, Nepal, & Wahid, 2016 studies climate projections over Koshi river basin applying delta approach as bias correction method on eight CMIP5 GCMs. Yet, the spatial

resolution used in these researches (~250 km) is too coarse to identify climate variations at scales required for environmental impact assessments, that is, 20-50 km (Wilby et al., 2000).

Ghimire et al., 2015 assessed the performance of CORDEX South Asia experiments for monsoonal precipitation over the Himalayan region, mainly, based on mean precipitation climatology over the region. Monthly, seasonal or longer averages obscure daily extremes in time series data while the daily information has a direct impact on human activities. Moreover, statistics like monthly or seasonal mean and standard deviation do not allow for a comparison of the entire data distribution on time scales of days (Perkins, Pitman, Holbrook, & McAneney, 2007) as daily extremes are averaged. Thus RCM simulations or the ensemble of RCMs with daily information should be used after bias corrections (Teutschbein & Seibert, 2010).

Very few researches (Perera et al., 2013, 2014) have been carried out over West Rapti river basin considering the climate projections and hydrological impact. Using bias corrected high resolution AGCM (20 km x 20 km) seems to offer promising representation of various micro-physical processes, however, the uncertainty associated with model parameters and internal model processes cannot be neglected.

1.4. Research Objective

The objective of this research is to assess uncertainty in streamflow estimates for a mountainous basin of regional scale in Nepal by uncertainty of climate change projections originating from a selection of downscaled Regional Climate Models (RCMs).

In this study, performance of different RCMs will be evaluated by use of gridded counterparts from the APHRODITE database to assess uncertainty by spread of RCM projections. Such spread results from use of different RCMs that are driven by specific initial conditions and lateral boundary forcing when downscaled from GCMs. The specific objectives of the research are outlined below:

- Compare and analyse spread of projections among CORDEX South Asia experiments
- Evaluate the effect of bias correction on RCM simulated precipitation and temperature
- Compare hydrological model simulated streamflow values with – and without – bias correction
- Assess uncertainty of simulated extreme streamflow events by RCM projections

1.5. Research Questions

1. What is the most appropriate set of RCMs that represent past climate, extreme climatic conditions and projected futures?

   This research question attempts to test the performance of RCMs over Nepal, and to identify set of RCMs, which closely simulate present and near-past climate and climatic extremes. Moreover, it is difficult to choose single best model by considering aspects of RCM model initialization. Hence, inclusion of all possible futures originating from different driving GCMs

is attempted here. These factors will help to assess the uncertainty originating from the spread of climate models' projections given by different RCMs.

2. How does the hydrological model perform for different RCMs, and bias corrected RCM simulations?

   Uncertainties related to climate change scenarios, and bias correction will be dealt with to understand the contribution of RCMs and bias correction to the overall uncertainty of the climate change induced impact assessment.

3. What are the impacts of predicted change in climate on peak and extreme low stream flows?

   This research question aims to evaluate the impact on peak and extreme low flows under medium and high impact-climate change scenarios.

1.6. Hypothesis

Spread of climate projections due to different RCMs driven by different GCMs leads to larger uncertainty in assessing impact of climate change on water resources.

2. STUDY AREA AND DATA

In section 2.1, study area is described separately for the whole Nepal as uncertainties in regional climate models has been studied for the entire country in section 2.1.1, and particular watershed information is discussed in section 2.1.2 with emphasis on hydrological impact of climate uncertainties. Available datasets for RCMs and observations are discussed in section 2.2.

2.1. Study Area

2.1.1. Nepal

Nepal has wide variation of climates from subtropical in the south, warm and cool in the hills, and cold in the mountains within a horizontal distance of less than 200 km. The remarkable differences in climatic conditions are primarily related to the enormous range of elevation within a short north-south distance. Generally, there are four seasons in Nepal: summer monsoon (June-September), post-monsoon (October-November), winter (December-February) and pre-monsoon (March-May). The climate at macro-level is dominated by the summer monsoon and topography plays an important role in creating meso- and micro-level differences. Hence, there are marked temporal and spatial variations in precipitation. The average area-weighted annual precipitation for Nepal is about 1,630 mm. More than 80% of the total annual precipitation occurs during the summer months. In extreme cases, up to 37% of the mean annual precipitation occurs within 24 hours. Mean annual precipitation ranges from only 163 mm in Lomangthang (Mustang) located in the trans-Himalayan zone north of the Higher Himalayan ranges, to more 5,000 mm in Lumle (Kaski) located in the southern part of the higher Himalayan ranges (Chalise & Khanal, 2001).

2.1.2. West Rapti River Basin

The West Rapti River (WRR) basin beholds immense importance concerning its significance in water supply for agriculture, irrigation, and domestic usage to the West Terai region of Nepal (Figure 1). Geographically, the study area extends from 27°56'50" to 28°02'30" North latitudes and 81°45'00" to 81°40'00" East longitudes. The length of main stream channel is 257 km. Originating from the Mahabharat range (middle mountains of about 3000 m altitude) of Nepal, it enters the lowlands and finally drains to Ghagra (Karnali) river, a tributary of Ganges River in India. Jhimruk River, Mari River, Arun River, Lungri River, Sit River, Dunduwa River, Sotiya and Gandheli rivulets are the main tributaries. The river is named West Rapti River at the downstream of confluence of Jhimruk and Mari rivers. Ground water and monsoon precipitation are the main contributors for water budget of river (Gautam & Phaiju, 2013).

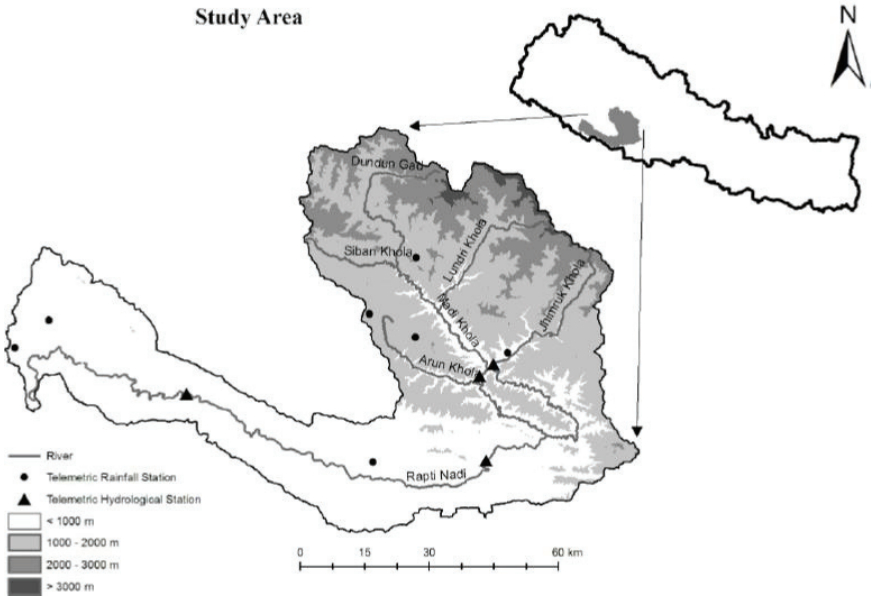

Figure 1 West Rapti River basin with hydro-meteorological stations and elevation information (Talchabhadel & Sharma, 2014)

Temperate climate prevails in the upper part of WRR basin while lower basin including Banke district has tropical to sub-tropical climate. . The period from March to May is hot and dry, June to August is hot and humid, September to October is pleasant, and November to February is cool and foggy with occasional rainfall due to westerly winds. In summer, the temperature reaches as high as 45 ^{0}C upstream while in winter, it falls below 2 ^{0}C downstream. Summer monsoon rainfall extends from June till September, and the basin receives about 80 percent of the total annual precipitation during monsoon only. The annual mean precipitation of the basin is about 1500 mm. The relative humidity ranges from 60 percent in May to above 90 percent in January (Gautam & Phaiju, 2013).

2.2. Datasets

2.2.1. CORDEX and its experiments

Coordinated Regional Climate Downscaling Experiment (CORDEX) program was set up under the support of World Climate Research Program (WCRP) to bring forth regional climate change scenarios globally. CORDEX South Asia constitutes of twelve different suites of experiment, and are available with the combination of different RCMs that are driven by different Global Climate Models (GCMs) initial and boundary forcing as shown in Table 2. RCMs information and output was obtained from CCCR website (*http://cccr.tropmet.res.in/home/aboutus.jsp*). Information on meteorological variables like daily maximum temperature (T_{max}), daily minimum temperature (T_{min}), daily mean temperature (T_{mean}) and precipitation (pr) are available at a horizontal resolution of 0.44 ^{0} (~50 km) spatial resolution with daily or monthly temporal resolution.

As mentioned in section 1.3 on the necessity of daily data to analyze the entire distribution of simulated variables, only RCMs with daily data was selected. In CORDEX South Asia experiments, only 7 out of 12 RCMs have daily data with historical, RCP 4.5 and RCP 8.5 information namely **RCA4 (ICHEC), CCAM (ACCESS), CCAM (CNRM), CCAM (CCSM), CCAM (MPI), CCAM (BCCR), and REMO 2009 (MPI)**. Hence, the study will focus on only these seven RCMs with historical or baseline period as 1976-2005 and future period as 2071-2100.

2.2.2. Observation Dataset

As *in-situ* station data suffers from poor spatial coverage and non-uniform distribution, use of daily gridded precipitation and temperature data are ever increasing to validate simulation of numerical models or satellite based products. Several such products exist like Asian Precipitation –Highly-Resolved Observational Daily Integration Towards Evaluation of Water Resources (APHRODITE), Global Precipitation Climatology Centre (GPCC), and Climatic Research Unit (CRU). Andermann, Bonnet, & Gloaguen, 2011 evaluated five different gridded precipitation data sets for Nepal, and found that APHRODITE offers the best precipitation estimates when compared to independent ground observations. Moreover, APHRODITE was capable to deliver adequate temporal variability at monthly and annual scale compared to other similar products, and authors further concluded that the product is appropriate for hydrological budget and discharge analysis.

APHRODITE's Water Resources data for monsoon Asia (60° - 150°E, 15° - 55°N) consists of daily gridded precipitation data (version V1101) for the period 1951 to 2007, and temperature data (version V1101R2) for the period 1961-2007 available at both 0.25^0 and 0.5^0 resolutions. These high resolution daily gridded datasets are outcomes of data collected from 5,000 – 12,000 stations (about two times more coverage than GPCC), with substantial improvement in depiction of areal distribution and variability of precipitation around the Himalaya compared to other available products (Yatagai et al., 2012). Therefore, APHRODITE climatic datasets were used to validate the historical outcomes of RCMs including input to the hydrological model.

Under Department of Hydrology and Meteorology (DHM), Government of Nepal, there are four hydrological stations at Kusum, Jalkundi, Bagasoti and Mari (Nayagaon). All the stations have real time telemetric system installed for water level measurement except for Bagasoti (real time rainfall measurement). The catchment area of the basins of Cherneta, Nayagaon, Bagasoti and Kusum gauging stations are 644 km^2, 1980 km^2, 3380 km^2 and 5200 km^2 respectively (Talchabhadel & Sharma, 2014). Except for Kusum, stations have more than 30 years of record of daily runoff information. Kusum station is at the lowest point of downstream with historical discharge information available from 2003 A.D. Since the records are not enough to evaluate climate change studies, station namely Jalkundi is used for this study with discharge information available from 1964 A.D. The hydrological information from this station was used during calibration and validation of hydrological model to match the model simulated discharge values.

Graphical plot of observed discharge from station Jalkundi along with gridded average temperature and precipitation values for the study basin from APHRODITE, and potential evapo-transpiration computed using Hamon's method is shown in Figure 2. Maximum average daily precipitation for the

basin is about 98 mm, yet, precipitation as high as 392 mm has be observed in the study area at daily time scale. Similarly, area-averaged temperature extends from 8 ^{0}C to 31 ^{0}C with average temperature of about 21 ^{0}C. Discharge at Jalkundi station has varied from as low as 1.11 cubic meter per second to 7196 cubic meter per second. The average discharge at the station is about 142 cubic meter per second. Potential evapo-transpiration computed using Hamon's approach with area-averaged temperature varies from 1.8 millimeter per day to 5.6 millimeter per day with average value of 1.84 millimeter per day.

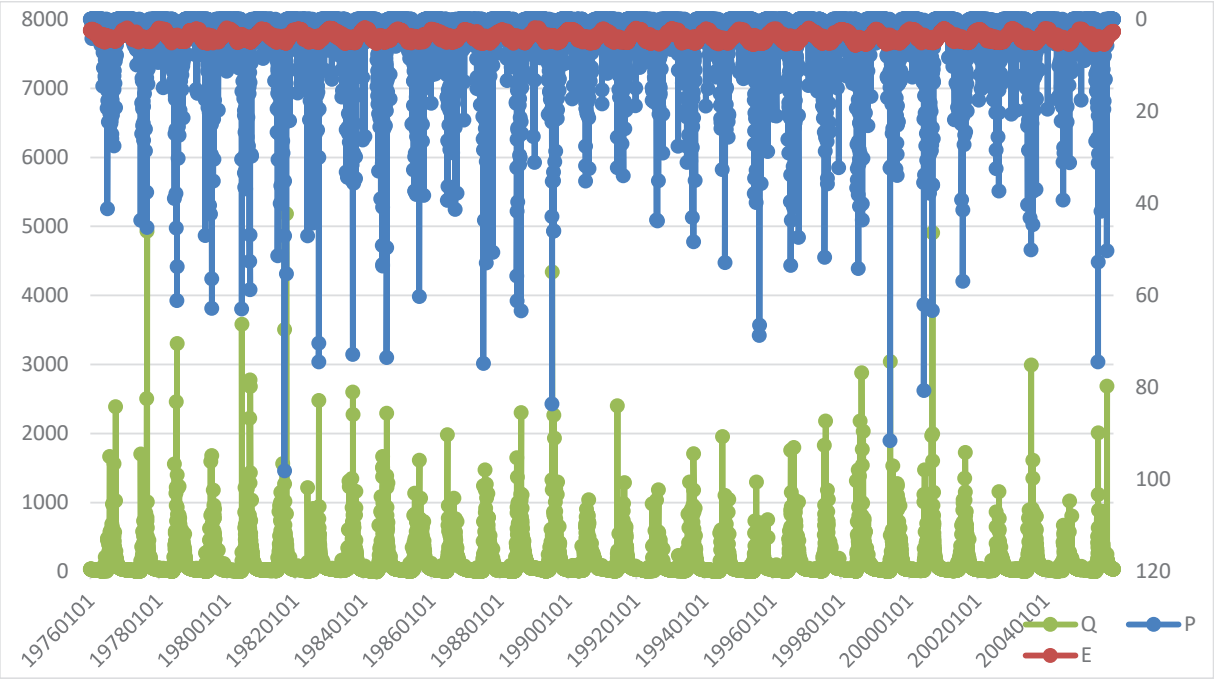

Figure 2 Graph showing observed discharge and precipitation, and computed potential evapo-transpiration

Table 2 List of CORDEX South Asia RCM experiments

Experiment Name	RCM Description	Driving GCM	Contributing Institute
CCLM4(MPI)	COnsortium for Small-scale MOdelling (COSMO) model in CLimate Mode version 4.8 (CCLM; Dobler and Ahrens, 2008)	Max Planck Institute for Meteorology, Germany, Earth System Model (MPI-ESM-LR; Giorgetta et al 2013)	Institute for Atmospheric and Environmental Sciences (IAES), Goethe University, Frankfurt am Main (GUF), Germany
RCA4(ICHEC)	Rossby Centre regional atmospheric model version 4 (RCA4; Samuelsson et al., 2011)	Irish Centre for High-End Computing (ICHEC), European Consortium ESM (EC-EARTH; Hazeleger et al. 2012)	Rosssy Centre, Swedish Meteorological and Hydrological Institute (SMHI), Sweden
CCAM(ACCESS)	Commonwealth Scientific and Industrial Research Organisation (CSIRO), Conformal-Cubic Atmospheric Model (CCAM; McGregor and Dix, 2001)	ACCESS1.0	CSIRO Marine and Atmospheric Research, Melbourne, Australia
CCAM(CNRM)		CNRM-CM5	
CCAM(CCSM)		CCSM4	
CCAM(GFDL)		GFDL-CM3	
CCAM(MPI)		MPI-ESM-LR	
CCAM(BCCR)		NorESM-M	
LMDZ4(IPSL)	Institut Pierre-Simon Laplace (IPSL) Laboratoire de Me´te´orologie Dynamique Zoomed version 4 (LMDZ4) atmospheric general circulation model (Sabin et al., 2013)	IPSL Coupled Model version 5 (IPSL-CM5-LR; Dufresne et al. 2013)	Centre for Climate Change Research (CCCR), Indian Institute of Tropical Meteorology (IITM), India
RegCM4(LMDZ)	The Abdus Salam International Centre for Theoretical Physics (ICTP) Regional Climatic Model version 4 (RegCM4; Giorgi et al., 2012)	IPSL LMDZ4	CCCR, IITM
RegCM4(GFDL)	ICTP RegCM4	Geophysical Fluid Dynamics Laboratory, USA, Earth System Model (GFDL-ESM2M-LR; Dunne et al. 2012)	CCCR, IITM
REMO2009(MPI)	MPI Regional model 2009 (REMO2009)	MPI-ESM-LR (Giorgetta et al 2013)	Climate Service Center, Hamburg, Germany

3. METHODOLOGY

This chapter discusses on the steps taken to accomplish the objective of this study. A synopsis of the research method is presented in Figure 3. This study is accomplished in five sequential steps with selection of representative concentration pathways (section 3.1), selection of representative regional climate models (section 3.2), bias correction (section 3.3), hydrological modelling (section 3.4) and extreme value analysis technique (section 3.5).

3.1. Selection of Representative Concentration Pathways (RCPs)

RCPs represent a set of four new pathways greenhouse gas (GHG) emission scenarios as a basis for long-term and near-term modeling experiments for the climate modeling community. These RCPs were developed considering different forcing agents like socio-economic scenarios, land use & cover data, emission data, and climate data. The four RCPs together span the range of year 2100 with radiative forcing values from 2.6 to 8.5 W/m^2 as presented in Table 3 (van Vuuren et al., 2011). Net effect of all anthropogenic GHGs and other forcing agents (except for land use – albedo, dust and nitrate aerosol forcing) are included in radiative forcing values. RCP 4.5 and RCP 8.5 are selected for this study to represent possible future by 2100 under medium stabilization and very high baseline emission scenarios respectively.

Table 3 Overview of RCPs

	Description
RCP 8.5	Rising radiative forcing pathway leading to 8.5 W/m2 (~1370 ppm CO2 eq) by 2100.
RCP 6	Stabilization without overshoot pathway to 6 W/m2 (~850 ppm CO2 eq) at stabilization after 2100
RCP 4.5	Stabilization without overshoot pathway to 4.5 W/m2 (~650 ppm CO2 eq) at stabilization after 2100
RCP 2.6	Peak in radiative forcing at ~3 W/m2 (~490 ppm CO2 eq) before 2100 and then decline (the selected pathway declines to 2.6 W/m2 by 2100).

Source: van Vuuren et al., 2011

3.2. Selection of Regional Climate Models (RCMs)

A regional climate model (RCM) is a numerical climate prediction model forced by specified lateral and ocean conditions from a general circulation model (GCM) or observation-based dataset (reanalysis) that simulates atmospheric and land surface processes, while accounting for high-resolution topographical data, land-sea contrasts, surface characteristics, and other components of the Earth-system (http://glossary.ametsoc.org/wiki/Regional_climate_model). As these RCM technique uses initial conditions, time-dependent lateral meteorological conditions and surface boundary conditions from GCMs, each RCM is likely to simulate different dynamically refined mesoscale climate features, reflecting the inherent and methodological uncertainties in climate modeling (Teichmann et al., 2013). Uncertainty in projections of climate has been reported by

several authors in South Asia and around the globe (Finger et al., 2012; Nepal, 2012; Syed, Iqbal, Syed, & Rasul, 2014; Ghimire et al., 2015; Alemseged & Tom, 2015; Rajbhandari et al., 2016).

To create further trustworthiness to climate change assessment, it is common to inter-compare projections from different RCMs. The method involves a three step sequential climate model selection procedure to develop representative climate projections among different RCMs for each RCP 4.5 and RCP 8.5 as proposed by Lutz et al., 2016.

Over the past decades, climate models have undergone major changes by substantial improvements to resolution, computations methods, parameterizations, and by considering additional processes like interactive aerosols in simulating many aspects of present climate. However, several limitations remain that mainly relate to representing clouds, which lead to uncertainties in the magnitude and timing, as well as regional details of predicted climate change (Randall et al., 2007) (Flato et al., 2013). Besides, RCPs are not final, fully integrated scenarios which means they do not represent a complete package of socio-economic, emission and climate projections (van Vuuren et al., 2011). Moreover, several systematic and random errors may originate due to imperfect conceptualization, discretization and spatial averaging within grid cells, and could result into models prediction with unusual and unrealistic large climate changes (i.e. outliers) (Hunt, 2007).

Considering the existing limitations of RCMs and RCPs, climate corners were defined based on temperature and precipitation, assuming that it would serve as a tool to address all possible climates. By the definition of extreme events that are in the outermost ten percent of the RCM simulation sample set, outliers were ignored from data analysis following *https://www.ncdc.noaa.gov/climate-information/extreme-events*. Thus, 10^{th} and 90^{th} percentile values were considered to set a plausible range of model outputs to represent variability of the phenomenon of interest while outliers in model simulations are ignored. Four corners of the climate spectrum were proposed in this study to represent plausible future climates. Once all the CORDEX experiments are brought under common data format and same resolution, 10^{th} and 90^{th} percentile values for relative changes in mean air temperature (ΔT) and annual precipitation sum (ΔP) between 1976 - 2005 (baseline period) and 2071 – 2100 (future period) are computed. Four corners of the spectrum of projections for temperature and precipitation change representing climates were defined based on these 10^{th} and 90^{th} percentile values. The tenth percentile value for ΔT and tenth percentile value for ΔP represents 'cold, dry' corner of the spectrum while tenth percentile value for ΔT and 90^{th} percentile value for ΔP denotes 'cold, wet' corner. Similarly 90^{th} percentile value for ΔT and tenth percentile value for ΔP represents 'warm, dry' corner, and 90^{th} percentile value for ΔT and 90^{th} percentile value for ΔP denotes 'warm, wet' corner of the spectrum (Table 4).

Table 4 Definition of climate corners

Criteria	Climate Corners
10^{th} percentile value for ΔT & 90^{th} percentile value for ΔP	cold, wet
10^{th} percentile value for ΔT & 10^{th} percentile value ΔP	cold, dry
90^{th} percentile value for ΔT & 90^{th} percentile value for ΔP	warm, wet
90^{th} percentile value for ΔT & 10^{th} percentile value ΔP	warm, dry

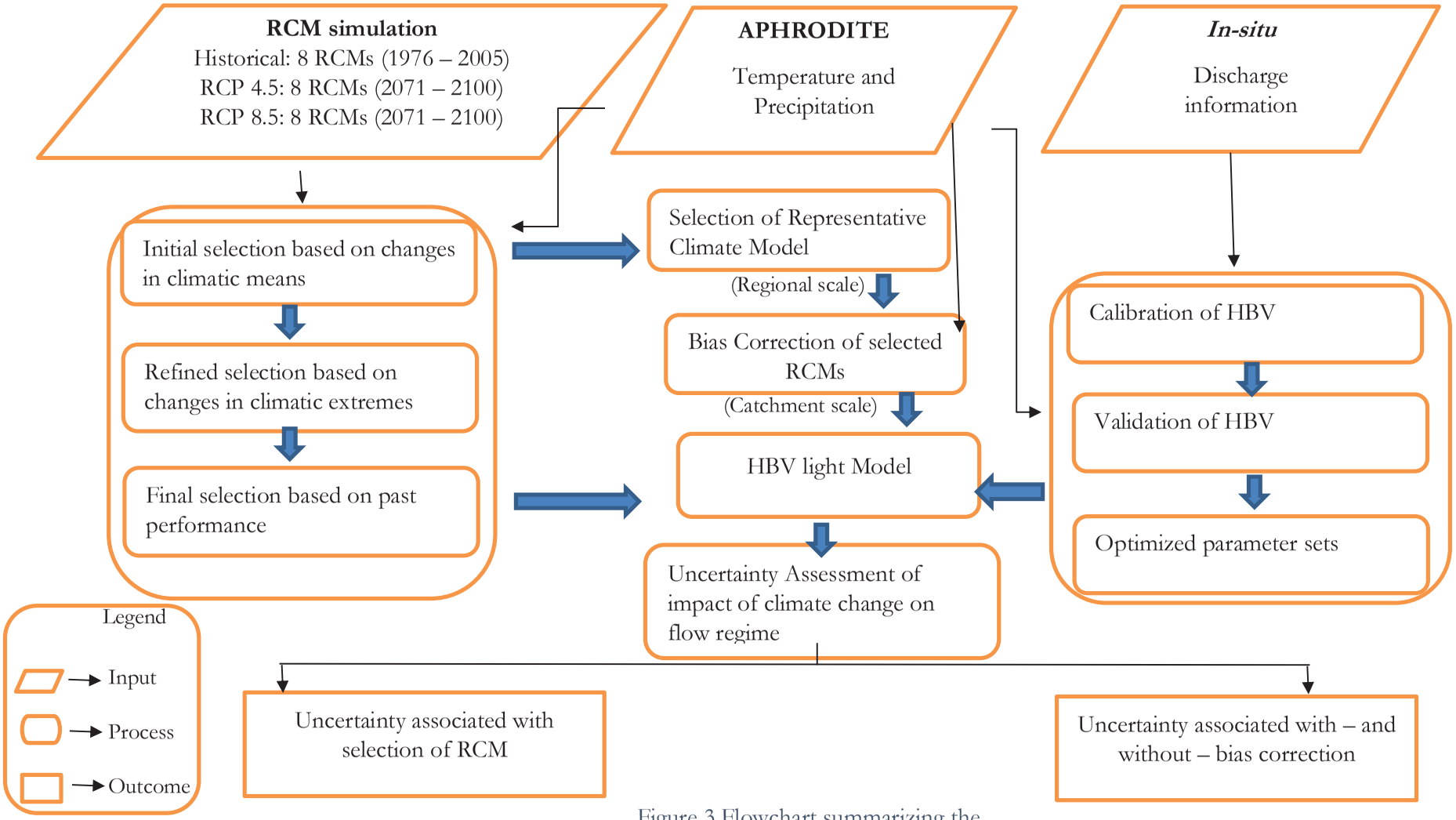

Figure 3 Flowchart summarizing the methods of this study

3.2.1. Selection of RCMs based on changes in climatic means

This step involving selection of RCMs is the first step of the three steps sequential-climate model-selection procedure, This step involved the selection of representative RCMs based on RCM simulated historical and future projections only, and it did not include any method of comparing the model simulated datasets with observations. This approach was considered with an attempt to represent projections of all RCMs that are subject to selected initial and boundary conditions. In addition, selecting a projection that best represents the future climate is rather subjective unless effects of initial and boundary condition are well defined to create plausibility of RCM model outcomes (i.e. climate projections). For this reason, it is common to consider multiple RCM runs by different initialization and different driving GCMs.

The 30-year time reference period from 1976-2005 (baseline or reference period) was analyzed and served as a reference for the future climate change simulations extending from 2071-2100 (future period). The differences in the climatological mean values of the future to the reference time period was used to define the climate change signals.

netCDF Operator toolkit (NCO) was used to manipulate and analyze data stored in netCDF format based Regional Climate Model (RCM) outputs. It served multiple purpose like arithmetic processing, attribute editing, binary operation, kitchen sinking, and record concatenating. GCM outputs from CSIRO only contained information on daily maximum temperature (T_{max}) and daily minimum temperature (T_{min}), thus NCO was utilized to compute daily mean temperature (T_{mean}). Similarly, units of precipitation (pr) and temperature were brought to common unit format, and it further required editing metadata to update the information. Similarly, each netCDF file contained unique variable data, and it was as huge as 1 GB. Hence, the tool was used to subset the file into study domain. Moreover, the files contained information at 5 years temporal scale. Thus, these files were concatenated into single file for reference and future period.

Thus obtained NetCDF format datasets for T_{mean} and pr was rasterized using R programming language and masked over shapefile of Nepal to obtain spatially averaged daily values of T_{mean} and pr over study area, Nepal. T_{mean} was averaged over the entire study period to obtain climatic means while daily pr values were accumulated to obtain total annual precipitation for each year, and further averaged.

Differences between 10th and 90th percentile values from the entire range of RCMs projections for ΔT and ΔP , and the corresponding projections of ΔT and ΔP from each models are calculated to measure the distance of the model to climate corners following Cartesian coordinate system and Pythagoras's theorem (Equation 1). ΔT and ΔP for each RCMs were plotted in x-axis and y-axis of scatterplot respectively to define each RCMs uniquely, along with climate corners. Thus, distance between climate corners and each RCMs were computed following Pythagoras's theorem.

$$Dp_i^T, p_i^P = \sqrt{\left(\left(\left|P_i^T - P_j^T\right|\right)^2 + \left(\left|P_i^P - P_j^P\right|\right)^2\right)} \qquad \text{Equation 1}$$

Where Dp_i^T, p_i^P is the distance of a model (j)'s ΔT and ΔP (P_j^T and P_j^P , respectively) to the corner (i)'s 10th and/or 90th percentile score of ΔT and ΔP for the entire ensemble (P_j^T and P_j^P , respectively).

Lutz et al., 2016 computed the distance between climate corners and each RCMs with the measurement units of ΔT and ΔP as ^{0}C and percentage respectively. However, in this study, coherence in the units of ΔT and ΔP was set up by computing relative changes in percentage for both variables.

The study by Lutz and team included 94 GCMs for RCP4.5 and 69 GCMs for RCP8.5 showing wide spread of projections, and offering greater opportunity to select representative GCMs over climate corners. However, this study could only use seven RCMs due to limited availability of RCMs under CORDEX South Asia, and necessity of daily data as explained in section 1.3. Thus, RCMs were repeatedly used to calculate distance from each corner. This may result into selection of same RCM at different corners, which is the limitation of this study. Thus, out of seven RCMs, only **five** RCMs with lowest values for Dp_i^T, p_i^P were selected for each corner, and sorted in ascending order. Hence, initial selection procedure leads to five model runs X four corners = 20 model runs for each RCP. In this step, five out of seven RCMs were chosen in order to maximize the inclusion of possible RCMs in each corner while filtering these models towards single best representative RCM in final step of selecting RCMs for each climate corners and each RCPs.

3.2.2. Refined selection of RCMs based on changes in climatic extremes

Frequency and severity of extremes largely define society's perception of climate variability and climate change. Thus, testing models' ability to simulate climate variability and extremes is an important part of model evaluation (Randall et al., 2007).

With an ultimate aim of detecting the changes in climate, Commission for Climatology (CCl) / World Climate Research Programme (WCRP) of World Meteorological Organization, project on Climate Variability and Predictability (CLIVAR) and Expert Team on Climate Change Detection, Monitoring and Indices (ETCCDMI) jointly recommended 27 climate change indices primarily focusing on extremes for climate change monitoring and detection studies. Out of these, 16 indices are temperature related, and 11 indices are precipitation related (Zhang X and Yang F, 2004).

Among these indices, warm spell duration index (WSDI) and cold spell duration index (CSDI) were considered for characterizing changes in air temperature extremes. WSDI is defined as number of days each year as a sequence of 6 or more days in which the daily maximum temperature exceeds the 90th percentile of daily maximum temperature for a 5 day running window surrounding this day during the study period (Eq. 2). Let Tx_{ij} be the daily maximum temperature on day i in period j and let $Tx_{in}90$ be the calendar day 90th percentile centred on a 5-day window (calculated using method from Appendix D). Then the number of days per period is summed where, in intervals of at least 6 consecutive days:-

$$Tx_{ij} > Tx_{in}90 \qquad \text{Equation 2}$$

Similarly, CSDI is defined as the number of days each year as sequence of 6 or more days in which the daily minimum temperature is below the 10th percentile of daily minimum for a 5 day running window surround this day during the study period (Eq. 3).

Let Tn_{ij} be the daily minimum temperature at day i in period j and let $Tx_{in}10$ be the calendar day 10th percentile centred on a 5-day window (calculated using the method from Appendix D). Then the number of days per period is summed where, in intervals of at least 6 consecutive days:-

$$Tn_{ij} < Tn_{in}10$$ Equation 3

Similarly, precipitation due to extremely wet days (R99pTOT) and consecutive dry days (CDD) were considered to characterize changes in precipitation extremes. CDD is defined as maximum number of consecutive days with precipitation less than 1 mm (Eq. 4). Let RR_{ij} be the daily precipitation amount on day i in period j. Count the largest number of consecutive days where:

$$RR_{ij} < 1mm$$ Equation 4

R99pTOT is defined as annual sum of precipitation in days where daily precipitation exceeds the 99th percentile of daily precipitation in the study period (Eq. 5). Let RR_{wj} be the daily precipitation amount on a wet day $w(RR \geq 1.0mm)$ in period j and let $RR_{wn}99$ be the 99th percentile of precipitation on wet days in the given period. If W represents number of wet days in the period, then:

$$R99p_j = \sum_{w=1}^{W} RR_{wj} \text{ where } RR_{wj} > RR_{wn}99$$ Equation 5

WSDI and CSDI affects the evapotranspiration while R99pTOT and CDD leads to associated hydrological extremes like flood and drought respectively. Importance of including climatic extremes in evaluating climate models is largely because extremes may change more than indicated by a change in the mean values. Moreover, impact models is very likely significantly dependent on the occurrence and frequency of extreme events.

For 'warm, wet' corner, WSDI and R99pTOT are considered as these indices best describe the corner of the spectrum. Similarly, WSDI and CDD are chosen for 'warm, dry' corner. Moreover, for 'cold, wet' corner, CSDI and R99pTOT are chosen, and for 'cold, dry' corner, CSDI and CDD are considered.

Climdex.pcic.ncdf package was used to read daily Tmax, Tmin, and pr in netCDF format, and construct the indices on annual basis for both baseline and future periods. Thus obtained extreme indices in netCDF format were rasterized using RStudio platform, and averaged over the study area. Furthermore, these annual (spatially averaged) indices were exported to excel to calculate average indices for baseline and future periods, and relative changes in indices in percentage between baseline and future period was computed.

Five RCMs initially selected based on climatic means are further refined based on their capability for their projected changes in climatic extremes for each RCP. The indices were calculated for both reference period and future period, and averaged over a period of 30 years. Percentual change for the future period with respect to the baseline period gives changes in the indices. These relevant indices were both ranked for each corner, and given scores 1-5. The model with the largest increase in indices scored five while the smallest increase scored 1. Thus, obtained scores were further averaged to give final score. Based on the final score for each corner, the three models with the highest score were selected. Thus, this step led to three models X four corners = 12 model runs for each RCP.

3.2.3. Final selection of RCMs based on past performance

Finally, the remaining models in each corner after the refined selection were validated against historical records from APHRODITE dataset to test performance of RCMs in simulating contemporary climates. Calculation of skill score of temperature were done based on metric proposed by Perkins et al., 2007. The metric calculates the cumulative minimum value of two distributions of each binned value, thereby measures the common area between two probability density functions (PDFs) as shown in equation 6. The skill score will equal one if a model simulates the observed conditions perfectly which is the total sum of the probability at each bin center in a given PDF.

$$S_{score} = \sum_1^n minimum(Z_{RCM}, Z_{OBS}) \quad \text{Equation 6}$$

Where n is the number of bins used to calculate the PDF for a given region, Z_{RCM} is the frequency of values in a given bin from the model, and Z_{OBS} is the frequency of values in a given bin from the observed data (Perkins et al., 2007).

RCMs and APHRODITE information in netCDF data format was converted to excel file format for each grid. Thus, dataset of each grid for observation and RCMs was read at a time, and sorted with the same range of values determined by range of observations. Bin size of 0.5 ^{0}C and 100 bins were used to create probability density functions. Finally, cumulative minimum value of two distributions at grid level was determined for all the grids to obtain Perkins skill score. Finally, these scores were further averaged over the study domain to obtain final score for each RCMs and RCPs refined from step 2 to obtain final representative RCM for each climate corner and RCPs.

E. Sanchez,R. Romera, M. A. Gaertner, 2009 proposed a method to score models from the comparison of precipitation cumulative density functions (CDFs) against observed values. It consists of five skill score factors f (i = 1, 5) considering variable behavior of precipitation of each model j (f_{ij}).

$$f_{1j} = 1 - \left(\frac{\left(|A_{RCM\,j} - A_{OBS}| \right)}{(2 * A_{OBS})} \right)^{0.5} \quad \text{Equation 7}$$

$$f_{2j} = 1 - \left(\frac{\left(|A^+_{RCM\,j} - A^+_{OBS}| \right)}{(2 * A^+_{OBS})} \right)^{0.5} \quad \text{Equation 8}$$

$$f_{3j} = 1 - \left(\frac{\left(|A^-_{RCM\,j} - A^-_{OBS}| \right)}{(2 * A^-_{OBS})} \right)^{0.5} \quad \text{Equation 9}$$

$$f_{4j} = 1 - \left(\frac{\left(|\overline{P_{RCM}}_j - \overline{P_{OBS}}| \right)}{(2 * \overline{P_{OBS}})} \right)^{0.5} \quad \text{Equation 10}$$

$$f_{5j} = 1 - \left(\frac{\left(|\sigma_{RCM\,j} - \sigma_{OBS}| \right)}{(2 * \sigma_{OBS})} \right)^{0.5} \quad \text{Equation 11}$$

$$W_j = f_{1j}.f_{2j}.f_{3j}.f_{4j}.f_{5j} \quad \text{Equation 12}$$

where $A_{RCM\,j}$, A_{OBS} are the areas below the j RCM and APHRODITE cumulative density function precipitation curves (equation 7), and A+ and A− are the fractional areas above (+) and below (−) the 50th percentile (equation 8 and 9). Overbar denotes the spatial and time average and σ the standard deviation of the probability distribution function (equation 10 and 11). Values of f_{ij} factors around 1 indicate that the RCM is close to APHRODITE observations, and values close to 0 mean that they are far from it. Each factor takes into account different aspects of model probability distribution characteristics: the distribution as a whole (through the mean and the total area), the smaller and higher precipitation amounts (50th percentile limit), and the shape of the distribution (through the variance). The final single-weight for each RCM $(W_{j)}$ was obtained by multiplying five factors for the model (equation 8).

Daily precipitation information from APHRODITE and RCMs in netCDF format was rasterized, and masked over the study area Nepal to obtain spatially averaged daily precipitation in excel format. Later, monthly precipitation values for each year was calculated for all RCMs and APHRODITE. From the range of datasets, maximum and minimum values were determined to distribute the whole range of datasets into 100 bins as proposed in the method to define bin size. Probability density functions was calculated for each bin for all RCMs and APHRODITE, and cumulative density functions were later obtained. Thus, five factors were multiplied to obtain final weight for the RCM.

Thus obtained skill scores for temperature and precipitation were averaged, and ranked in ascending order. Finally, one model runs X four corners = four model runs will be used for each RCP in hydrological impact assessment under climate change.

3.3. Bias correction

This study utilizes the RCM outputs based on dynamical downscaling of GCMs which improves the representation of regional features in climate projections. However, local inaccuracies owing to insufficient resolution and the uncertainties in the representation of small-scale forcing and processes like clouds, convection, boundary layer, radiative transfer, etc exist. In general, two straight forward corrections include adding the difference between climatological means of RCM simulated future and baseline period to an observed baseline (delta approach). This technique is based on an assumption that variability in climate scenario remains unchanged (Amengual, Homar, Romero, Alonso, & Ramis, 2012). This study adopts quantile-quantile mapping transformation (empirical quantile mapping) as it is more flexible that delta approach, and amends mean, variability, and shape errors in simulated cumulative distribution functions (CDFs) of climatic variables.

3.3.1. Empirical Quantile Mapping

It involves calculation of changes in CDFs of daily RCM outputs between baseline and future period quantile by quantile. This is further rescaled based on observed CDF for the same baseline period, and then added, quantile by quantile, to the observation dataset to obtain new calibrated future CDFs (Amengual et al., 2012). This is expressed as

Difference between RCM simulated raw baseline period values (s_{ci}) and raw future period values (s_{fi}) of precipitation and temperature for ith quantile value of CDF is calculated (equation 13). Thus, it offers quantile by quantile changes (Δ_i) in the CDFs. Here, the term 'raw' represents the RCM simulated values without any bias-adjustment. Similarly, mean value of RCM simulated raw baseline period ($\overline{S_c}$) and future period values ($\overline{S_f}$) are calculated to obtain mean changes ($\overline{\Delta}$) in the values (equation 14). Furthermore, difference (Δ'_i) between $\overline{\Delta}$ and Δ_i is calculated (equation 15) to obtain quantile by quantile changes in CDFs, and finally added to APHRODITE values (o_i) quantile by quantile to obtain bias-adjusted calibrated future values (p_i) (equation 16) as shown in Figure 4.

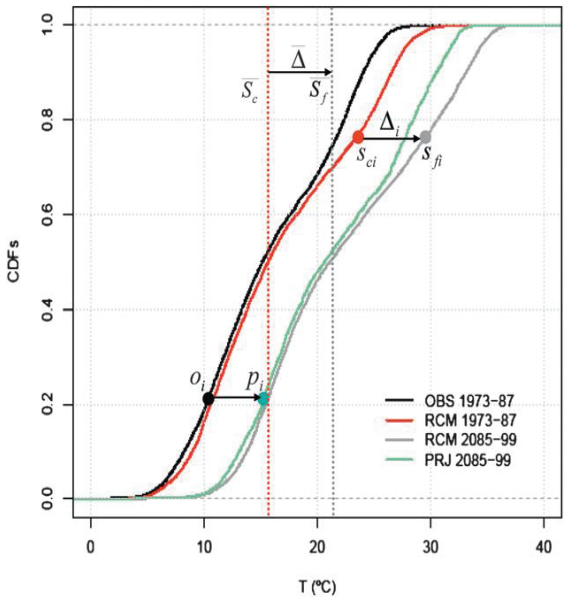

Figure 4 Graphical Sketch of Q-Q adjustment

Source: (Amengual et al., 2012)

$$\Delta_i = s_{fi} - s_{ci} \quad \text{Equation 13}$$

$$\overline{\Delta} = \overline{S_f} - \overline{S_c} \quad \text{Equation 14}$$

$$\Delta'_i = \Delta_i - \overline{\Delta} \quad \text{Equation 15}$$

$$p_i = o_i + \overline{\Delta} + \Delta'_i \quad \text{Equation 16}$$

Simulated CDFs for future period is calibrated by adding to the observed quantile, both mean delta change, and individual delta changes in the corresponding quantiles.

3.4. Hydrological Model

Hydrological models have increasing wide range of applications like water resources planning, development and management, flood prediction, and coupled systems modeling like water quality, hydro-ecology and climate (Pechlivanidis, Jackson, Mcintyre, & Wheater, 2011) along with future system response modeling, for example, climate and land use changes to reproduce the water balance of the study area. The major advantage of these models in the field of water resource management is simulation of hydrological behavior with limited spatial and temporal information on catchment characteristics, meteorological forcing, and land cover information.

3.4.1. HBV Light Model

HBV model has been widely used by several researchers to assess the impact of climate change on water resources (Abdo, Fiseha, Rientjes, Gieske, & Haile, 2009; Teutschbein & Seibert, 2012; Nigatu, 2013). HBV model named after Hydrologiska Byrans Vattenavdelning unit at the Swedish

Meteorological and Hydrological Institute (SMHI) was first developed in 1970s. Since then, several progresses have been made until now and its popularity is mainly due to the simple and robust structure, and a small number of parameters. HBV model is, a semi-distributed, widely-used conceptual model with possibility to run simulations with different time steps and several sub-catchments and elevation zones. The model consists of different routines and simulates catchment discharge, usually on a daily time step, based on time series of precipitation and air temperature as well as estimates of monthly long-term potential evaporation rates (Seibert & Vis, 2012).

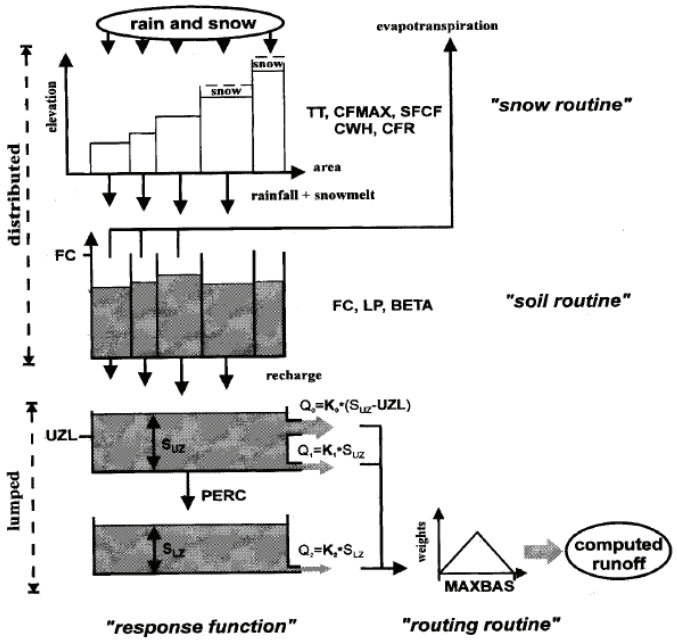

Figure 5 Structure of HBV model Source: (Seibert, 2000)

The basic-standard version of the model (with use of UZL) consists of three main modules: snow accumulation and melt, soil moisture accounting and river routing and response modules (Figure 5). The soil moisture accounting routine, which is controlled by three parameters, computes an index of the wetness and soil moisture storage in a catchment. Parameter FC is the maximum soil moisture storage capacity in the basin and parameter BETA determines the relative contribution to runoff from a millimetre of rain or snowmelt at a given soil moisture deficit while parameter LP is a soil moisture value above which AET reaches PET, and controls the shape of the reduction curve for potential evapotranspiration. The response routine transforms excess water from the soil moisture routine to discharge to each sub-basin. It consists of two reservoirs connected in series by constant percolation rate PERC. The routine has three recession coefficients, namely K0, K1 and K2, a reservoir threshold UZL, and a constant percolation rate PERC. Computed outflow from a catchment is transformed using a triangular weighting function, the base width of which is the calibration parameter MAXBAS. The transformed catchment response is routed with a Muskingum routing model (Abebe, Ogden, & Pradhan, 2010). *In-situ* discharge information will be used for model calibration and validation of the model.

3.4.2. Estimation of Potential Evapotranspiration

HBV model requires daily temperature, precipitation and potential evapo-transpiration (PET) values as driving variables. Temperature and precipitation information are available from APHRODITE and RCM outputs. However, PET values are to computed or derived from available datasets. For this purpose, different methods like Thornthwaite, Hamon, Hargreaves-Samani, Priestley-Taylor, Ture, Makkink, Penman-Monteith, etc to estimate PET exist, however, choice of methods largely differs the results (Cruff & Thompson, 1967; Rao, Sun, Ford, & Vose, 2011). Based on available datasets of temperature and precipitation only for calculating daily PET, and findings by Lu, Sun, McNulty, & Arnatya, 2005 that Hamon method gives better estimate, when only temperature data is available, this study uses Hamon method to estimate PET.

The Hamon method computes PET as a function of daily mean air temperature and hours of sunshine (Bae et al., 2011). Solar declination (d) is calculated based on Julian day (J) of each day for entire period (equation 17), and sunset solar angle (Ω_s) is determined based on Ld, and representative latitude of the catchment (φ) as shown in equation 18. Number of hours of sunshine for each day (ω) is computed based on sunset solar angle (equation 19). Mean air temperature (T) from APHRODITE is used to calculate saturated vapor pressure (ESAT) as in equation 20, and thus vapor density (RHOSAT) for the given temperature (equation 21). Finally, PET is calculated based on daytime length of sunshine and saturated vapor density, along with calibration coefficient KPEC which is set to 1.2 as proposed by Lu et al., 2005 (equation 22).

$$Ld = 0.4093 * sin\left(\frac{2*J*\pi}{365} - 1.405\right) \quad \text{Equation 17}$$

$$\Omega_s = acos\left(-tan\left(\frac{2*\pi*\varphi}{360}\right) * tan\, d\right) \quad \text{Equation 18}$$

$$\omega = \frac{24*\Omega_s}{\pi*12} \quad \text{Equation 19}$$

$$ESAT = 6.108\ x\ EXP\ (17.26939\ x\ T\ /\ (T + 237.3)) \quad \text{Equation 20}$$

$$RHOSAT = 216.7\ x\ ESAT\ /\ (T + 273.3) \quad \text{Equation 21}$$

$$PET = 0.1651 * \omega *\ RHOSAT\ x\ KPEC \quad \text{Equation 22}$$

3.4.3. Model Calibration

Model calibration refers to the re-adjustment and re-calculation of parameter values to find the best fit or in other words, it also refers to finding the optimum value of objective function (Rientjes, 2015). A numerical measure of the difference between the model simulated output and the observed (measured) catchment output is objective function (or goodness of fit). A popular objective function in the hydrological literature is the Nash-Sutcliffe Efficiency (NSE) criterion (equation 10), which gives the proportion of the variance of the data explained by the model (Nash & Sutcliffe, 1970). Moreover, Liu & Smedt, 2004 proposed NSE adapted for low flow conditions (LNSE) and for high flow conditions (HNSE) as shown in equations 11 and 12 respectively.

$$NSE = 1 - \left[\frac{\sum_{i=1}^{n}(Q_{sim} - Q_{obs})^2}{\sum_{i=1}^{n}\left(Q_{sim} - Q_{mean}^{obs}\right)^2}\right] \quad \text{Equation 23}$$

$$LNSE = 1 - \left[\frac{\sum_{i=1}^{n}[ln(Q_{sim}) - ln(Q_{obs})]^2}{\sum_{i=1}^{n}[ln(Q_{obs}) - ln(Q_{mean}^{obs})]^2}\right] \quad \text{Equation 24}$$

$$HNSE = 1 - \left[\frac{\sum_{i=1}^{n}(Q_{obs} + Q_{mean}^{obs})(Q_{sim} - Q_{obs})^2}{\sum_{i=1}^{n}(Q_{obs} + Q_{mean}^{obs})(Q_{obs} - Q_{mean}^{obs})^2}\right] \quad \text{Equation 25}$$

Where Qobs is the observed stream flow [L^3T^{-1}], Qsim is the simulated stream flow [L^3T^{-1}], Q^{obs}_{mean} is the mean of the observed stream flow [L^3T^{-1}] and ϵ is an arbitrary chosen small value to avoid problems with nil observed or simulated discharges.

4. RESULTS

This chapter presents the findings of the methods adopted from chapter 3. Uncertainty analysis of choice of RCMs are discussed in section 4.1. This section further deals with the analysis of RCM outputs based on climatic means, extreme indices, and observed datasets. Results of RCM outputs with and without bias correction is presented in section 4.2. Uncertainty in climate projections is discussed further in section 4.3. Results of calibrating and validating HBV model and future projections of discharges with- and without-bias correction are discussed in section 4.4 and 4.5 respectively. Finally, the analysis of extreme low flows and high flows are presented in section 4.6.

4.1. Selection of Regional Climate Models (RCMs)

4.1.1. Selection of RCMs based on changes in climatic means

Figure 6 shows box-whisker plot that represent the absolute changes in monthly temperature for the future period relative to the baseline period (ΔT) for all RCMs and RCPs. The bars in the middle of the boxes denote the median values, and the upper and lower boundaries of the boxes show the 75th and 25th percentiles, respectively and the distance between those two is inter quartile range (IQR). Cross marks denotes mean value. Whiskers represent minima and maxima changes which are maximum 1.5 times the IQR above 75th percentile or below 25th percentile; changes outside this range are represented as outliers (Hubert & Vandervieren, 2008). The ticks outside of the boxes denote the maximum and minimum values of dataset.

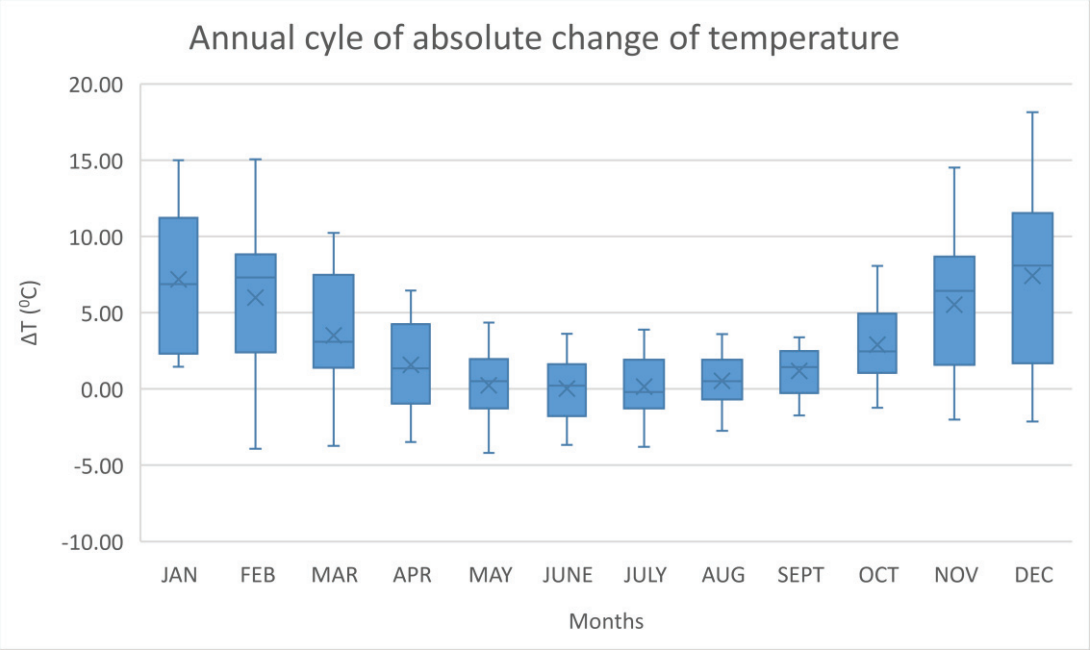

Figure 6 Whisker plot on delta air temperature for all RCMs and RCPs

Mean absolute changes in monthly temperature shows positive changes which indicates warming of the overall climate by the end of 21st century. March, April and May represent pre-monsoon, and monsoon extends from June till September. It indicates that pre-monsoon will be warmer than monsoon period. Similarly, winter months (December, January and February) shows the highest tendency towards warmer climate. It further suggests that rise of temperature in future period will

be higher for winter compared to summer. Mean ΔT values are lowest for June (0.04 ^{0}C) and highest for December (7.41 ^{0}C). Inter-quartile range (IQR) of entire months shows that there is larger relative dispersion of the middle 50 % of ΔT. Moreover, IQR is smaller for the monsoon period with higher value for the remaining months. Relative dispersion of dataset-outer range at 75th percentile to maximum is greater compared to minimum to 25th percentile, it also indicates warmer climate towards the end of this century.

For winter, IQR is relatively small compared to the whisker range which suggest clustering of data about the median with longer tails representing large dispersion of the relative extreme values. December has the largest IQR for ΔT with minimum for August. Minimum values near to 25th percentile shows the little difference of extremes from the remainder of the sample. Except for January, minimum values of absolute changes of temperature have negative values, which are very small compared to maximum values, and it ranges from -4.2 ^{0}C (May) to -0.27 ^{0}C (September). Maximum values farther away from the 75th percentile shows marked difference of extremes from the remainder sample. It further explains the tendency of larger changes in ΔT which is highest (18.5 ^{0}C) for the month December, and lowest (3.39 ^{0}C) for the September. It further shows that December will have largest absolute changes in temperature.

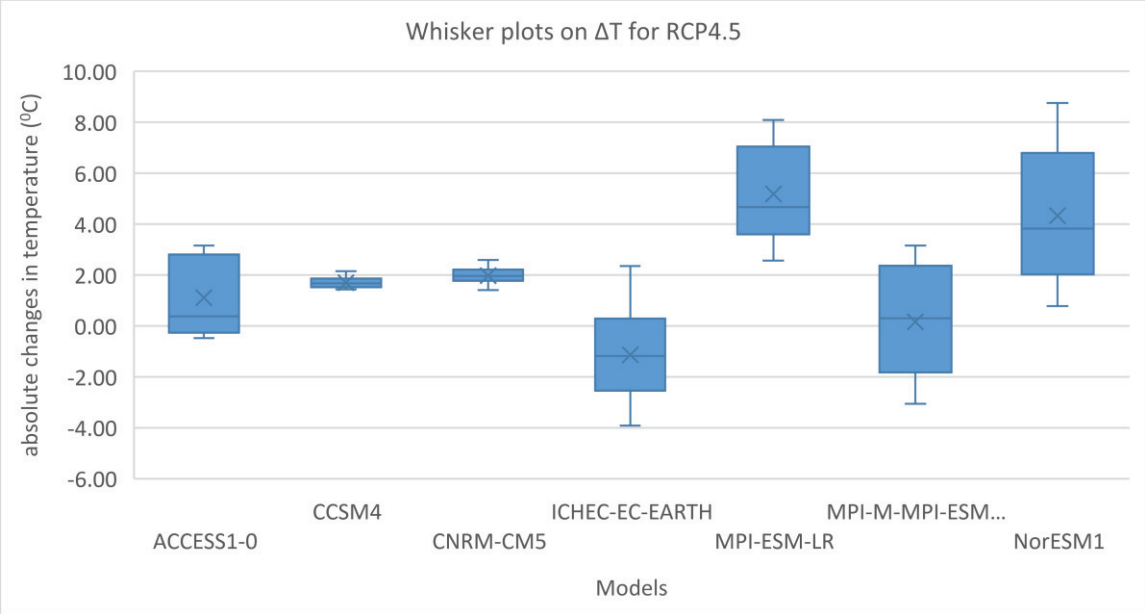

Figure 7 Whisker plot of ΔT for RCP 4.5

Changes in temperature (ΔT) for each of the RCMs and RCPs were further prepared as shown in Fig 7 & 8 respectively. Mean values of ΔT in Figure 7 shows that all the models showed positive changes towards warmer climate by the end of century compared to baseline period, except for ICHEC-EC-EARTH. IQR for CCSM4 and CNRM-CM5 show very little relative dispersion of middle 50 percent of ΔT, and it is highest for NorESM1. Maximum values of ΔT show the overall increment of temperature which ranges from 2.15 0C (CCSM4) to 8.76 0C (NorESM1).

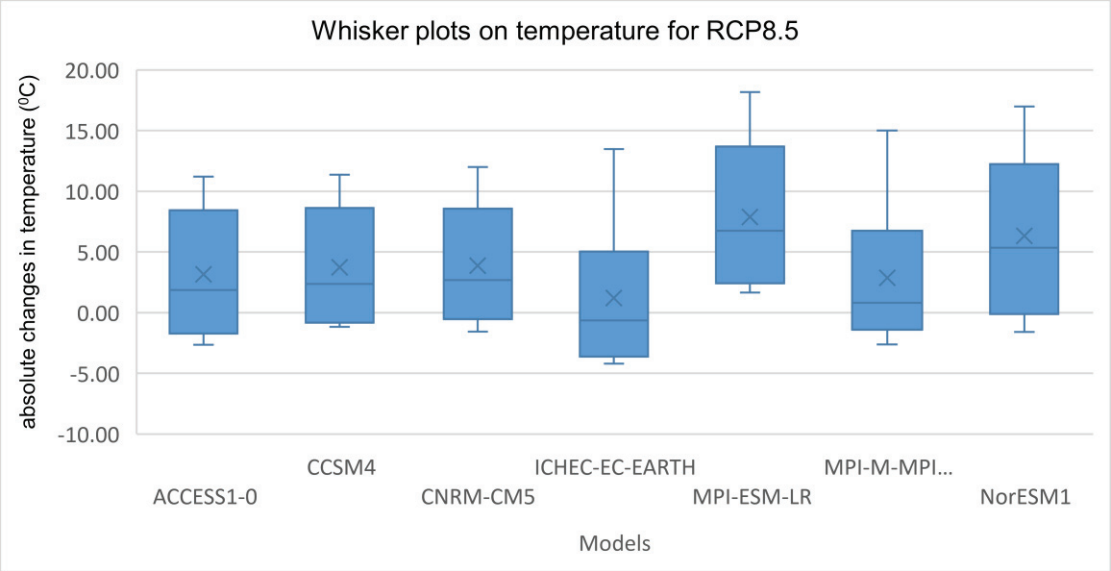

Figure 8 Whisker plot of ΔT for RCP 8.5

Figure 8 explains the whisker plot of ΔT for RCP8.5, and mean values of ΔT show warmer climate for all RCMs. It ranges from 1.21 ^{0}C (ICHEC-EC-EARTH) to 7.37 ^{0}C (MPI-ESM-LR). Moreover, mean values above the median further supports the warmer climate. Relative dispersion of whiskers show the higher tendency of ΔT values greater than 75th percentile. NorESM1 has the largest dispersion of the middle 50 percent of dataset with least for ICHEC-EC-EARTH.

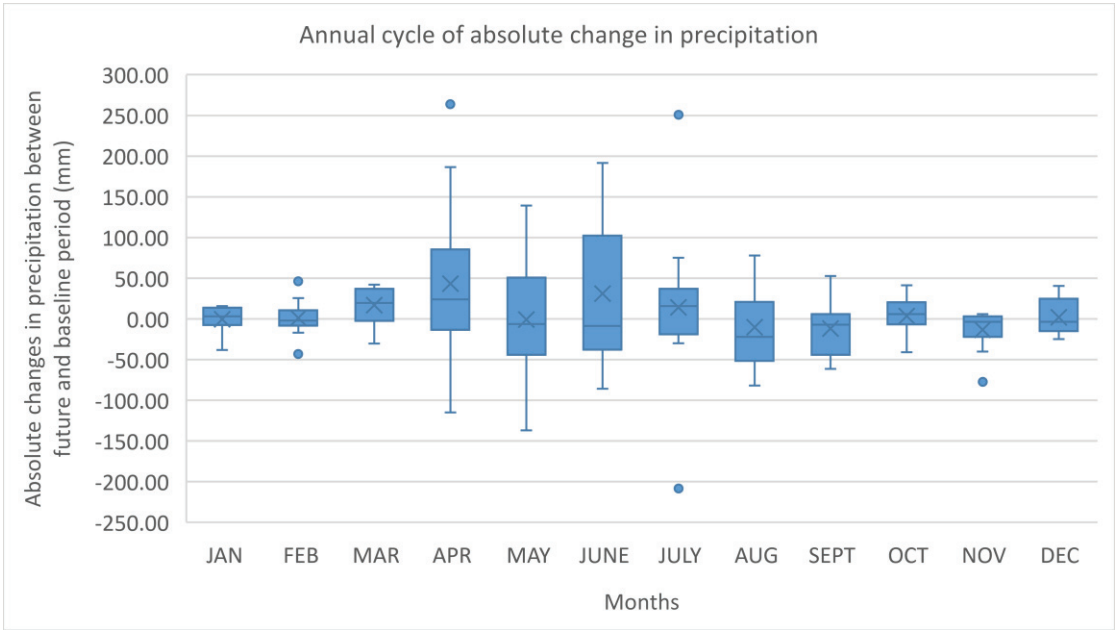

Figure 9 Whisker plot of absolute change of precipitation amount for all RCMs and RCPs

Projected absolute changes in monthly precipitation (ΔP) between baseline (1976-2005) and future time period (2071-2100) for all RCMs and RCPs are shown in Figure 9. Relative changes ranges from -136 mm (May) to 191 mm (June). The figure indicates the shifting of precipitation from monsoon to pre-monsoon months as April and May have relatively higher increment of precipitation compared to July, August and September. Inter quartile range for summer months

(monsoon period) shows the less changes with larger negative precipitation in future period compared to baseline period except for July. However, whiskers towards maximum values are longer compared to whiskers towards minimum values, and it signals towards extreme precipitation events. During post-monsoon (October and November), not much variability in precipitation can be observed while in winter, December seems to have increased precipitation while January and February show little variability. In reference to Figure 6 which shows the warmer temperature in winter, it can be concluded that winter months are very likely to suffer from drought at the end of century.

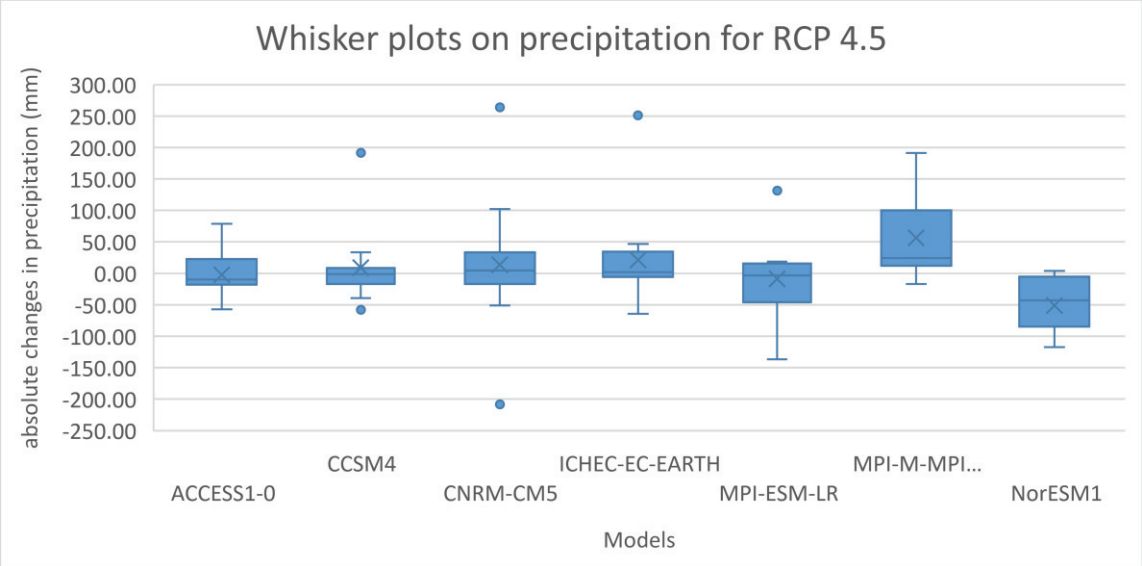

Figure 10 Whisker plot of absolute change of precipitation amount for RCP 4.5

Figure 10 shows the model output of each RCMs for RCP 4.5 with ΔP ranging from -136 mm (MPI- ESM-LR) to191 mm (MPI-M-MPI-ESM-LR). Mean absolute changes in precipitation shows mixed results as ACCESS1-0, MPI-ESM-LR and NorESM1-M indicate decrease in mean values while remaining models shows increased mean changes in precipitation. Compared to temperature results, precipitation shows greater variability as whiskers towards maximum values are higher for ACCESS1-0, CNRM-CM5, and MPI-M-MPI-ESM-LR indicate towards heavy precipitation events in future, while remaining models indicate towards less precipitation. NorESM1 shows the overall decrease of precipitation including MPI-ESM-LR. ICHEC-EC-EARTH does not indicate much change in total amount of precipitation as the median value for ΔP is near to zero, yet the lower whisker also indicate towards possible drought in future.

Similarly, absolute changes in precipitation values between baseline and future period for each RCMs were explored for RCP8.5 as shown in Figure 11. Mean values of changes in precipitation is above zero except for MPI-M-MPI-ESM-LR, which indicates towards increase in precipitation in future period. All RCMs show common pattern that the maximum precipitation is very likely to increase while the minimum values are decreasing. It further confirms the likelihood of heavier precipitation. Changes in minimum values range from - 51.49 mm (NorESM1) to -11.88 mm for ICHEC-EC-EARTH. And, maximum values range from 34.87 mm (CCSM4) to 139.14 mm (NorESM1). NorESM1 shows the largest variability in predicting future period based on IQR and whiskers, while MPI-M-MPI-ESM-LR shows the least variability.

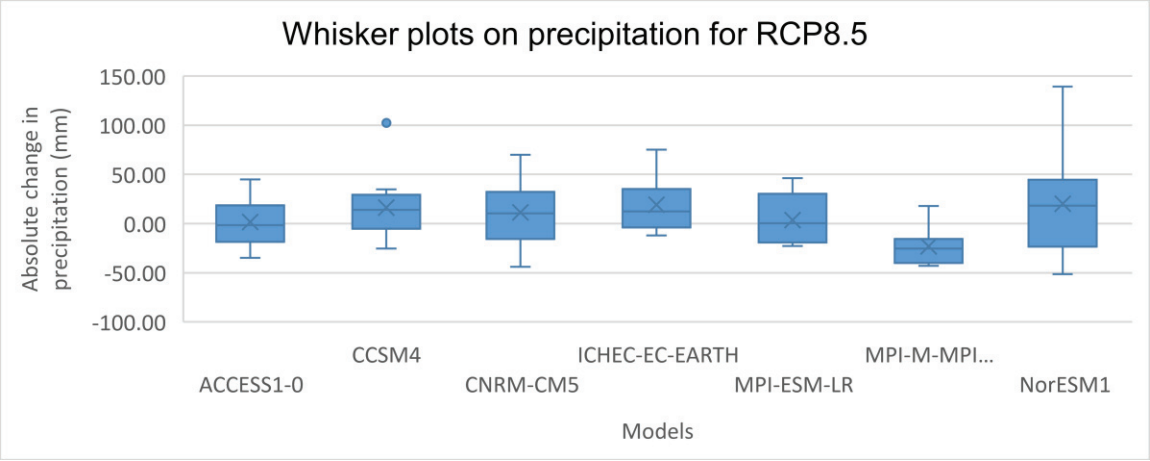

Figure 11 Whisker plot of absolute change of precipitation amount for RCP 8.5

Distance of each RCM runs to the 10th and 90th percentile values in the corners were calculated (Equation 1), and ranking of these models for each corner was performed starting from the least one. Five RCMs with the least distance between each climate corners and each RCMs were selected for further analysis to calculate the extreme indices for each climate corners and each RCPs. The red squares in scatter plots (Figure 12 and 13) shows the climatic corners as described in Table 4. These scatter plots explain that larger number of RCMs are clustered around COLD, WET corner of the climate corners. The scale of distribution of ΔT and ΔP values in RCP 4.5 and RCP 8.5 further proves the outcomes of radiative forcing pathways on severity of possible climate changes respectively as the values of ΔT and ΔP for RCP8.5 are almost twice compared to RCP4.5. COLD, DRY corner do not show any closeness to available RCMs. ICHEC-EC-EARTH shows closeness towards WARM, WET corner, and MPI-M-MPI-ESM-LR shows closeness towards WARM, DRY corner. These results from scatter plot could be influenced by limited availability of RCMs to represent climatic diversity for the study.

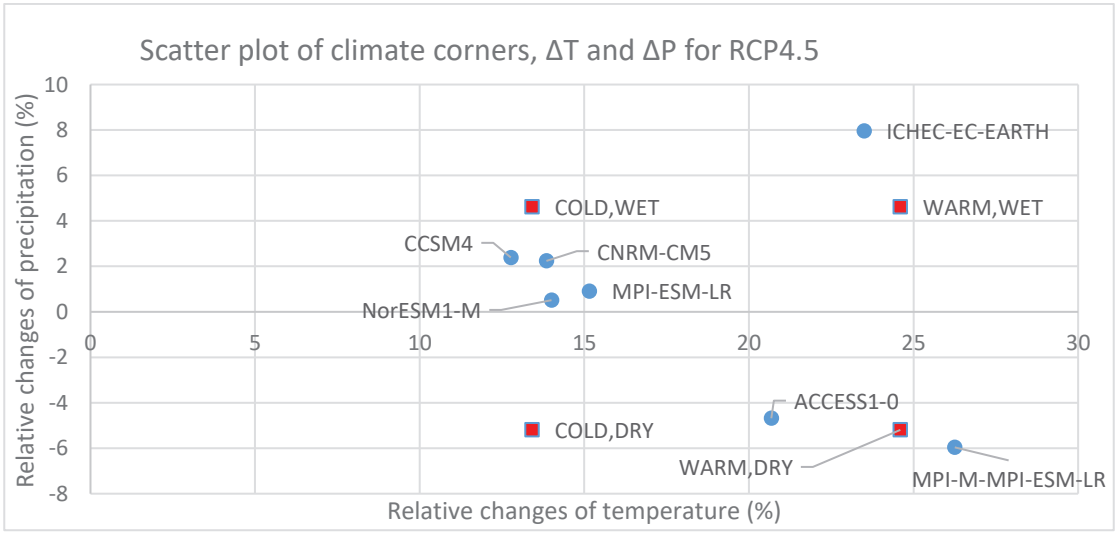

Figure 12 Scatter plot of climate corners, ΔT and ΔP for RCP4.5

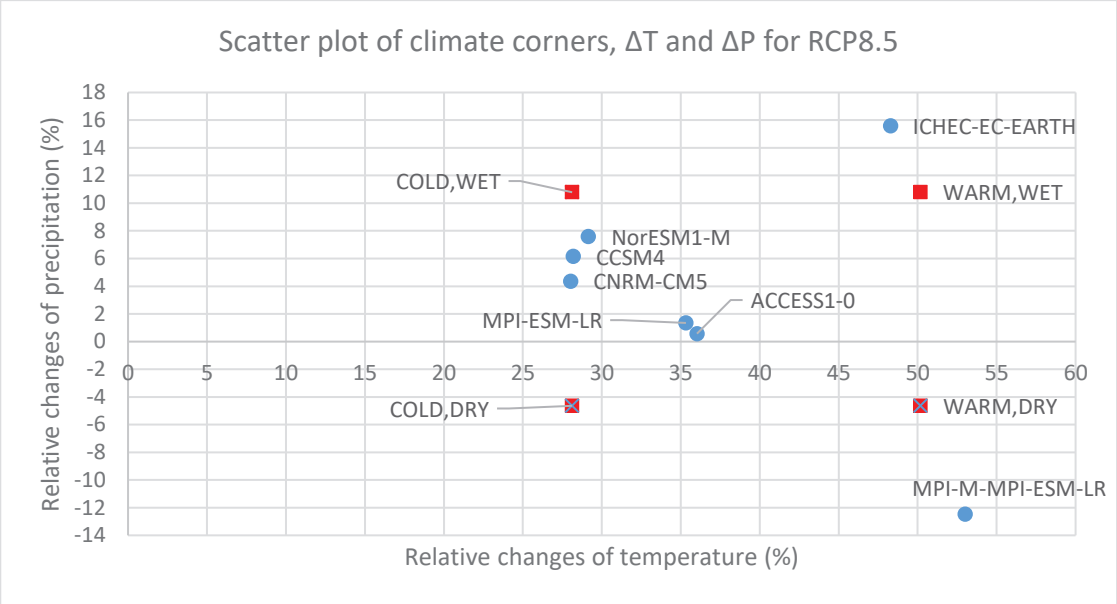

Figure 13 Scatter plot of climate corners, ΔT and ΔP for RCP8.5

Results of distance calculation for RCP 4.5 and RCP 8.5 are shown in Figures 14 and15 respectively. RCMs with least distance were selected for each climate corner for extreme indices analysis.

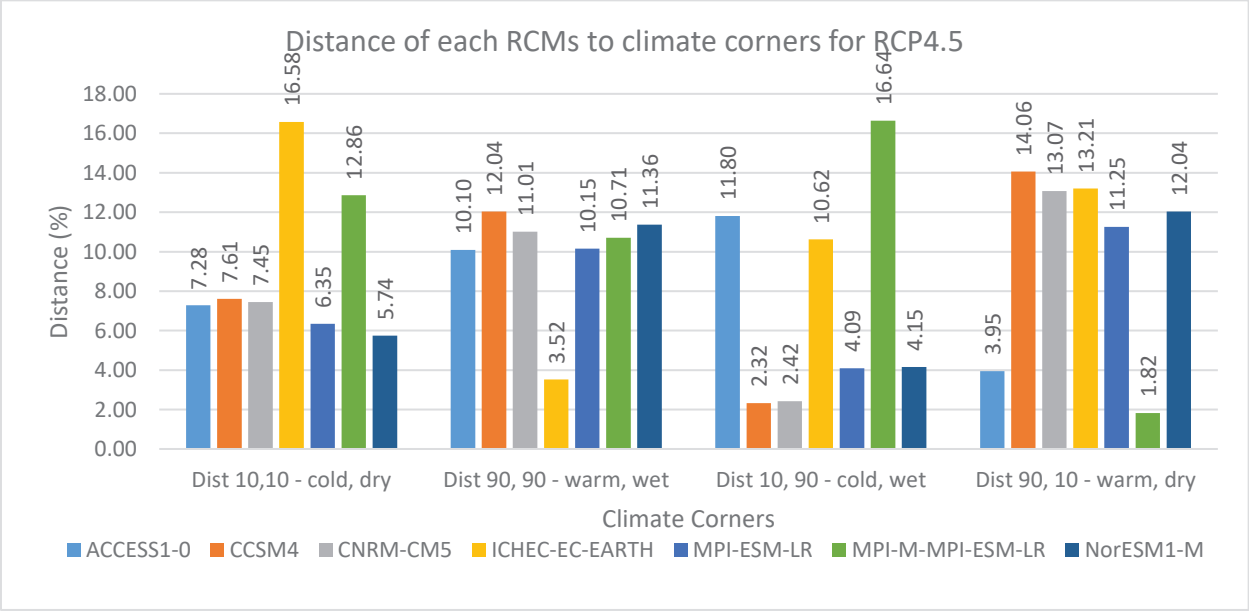

Figure 14 Distance of each RCMs to climate corners for RCP4.5

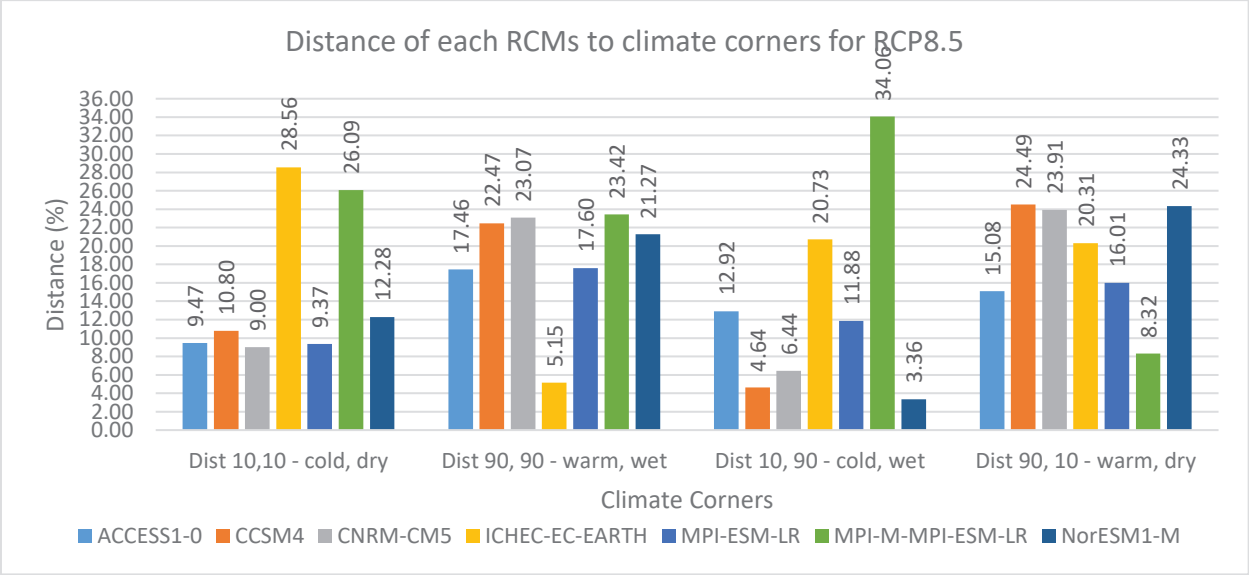

Figure 15 Distance of each RCMs to climate corners for RCP8.5

4.1.2. Refined selection of RCMs based on changes in climatic extremes

Relative change of extreme indices between 1976-2005 and 2071-2100 was obtained (Figure 16). Bar plots were prepared to plot the relative changes of indices against each RCMs. Figure 16a on consecutive dry days (CDD) indicates the decreasing trend at the end of 21st century for all the models except for MPI-M-MPI-ESM-LR . It ranges from -23 percent (CCSM4, RCP8.5) to 60 percent (MPI-M-MPI-ESM-LR, RCP8.5). MPI-M-MPI-ESM-LR and ACCESS1-0 show the greatest variation for both RCPs respectively. CNRM-CM5 and ICHEC-EC-EARTH show different behavior as the changes in RCP4.5 are higher compared to RCP8.5. CSDI (Fig 16b) shows mixed response by different RCMs, especially with choice of RCPs. RCP4.5 and RCP8.5 have opposite results for CCSM4, CNRM-CM5, MPI-M-MPI-ESM-LR and ACCESS1-0. And, all RCMs except for CCSM4 show increasing trend of CSDI for RCP8.5 which ranges from -6.22 percent (CCSM4) to 63 percent (MPI-ESM-LR). These results are in line with Fig 1, which showed the negative changes of minimum values of absolute changes between future period and baseline period.

Figure 16c explains WSDI, and models show non-consistent responses. ACCESS1-0, CCSM4, CNRM-CM5, and ICHEC-EC-EARTH indicate negative changes, which means number of days of warm spell will decrease in future period with reference to baseline period. Figure 12 and 13 showing scatter plots of RCMs in different climate corners for RCP 4.5 and RCP 8.5 respectively also show similar results. MPI-ESM-LR and MPI-M-MPI-ESM-LR show positive trend of WSDI in future period, and it ranges from 0.17 percent to 18.82 percent.

All the models exhibit positive trend towards extremely heavy precipitation events (R99PTOT) by the end of century except for MPI-M-MPI-ESM-LR for RCP85 and ICHEC_EC_EARTH (Figure 16d). For the remaining models, RCP85 shows extreme weather conditions compared to RCP 45 ranging from 6.4 percent (MPI-ESM-LR, RCP45) to 21.22 percent (ACCESS1-0, RCP85). This further confirms with Figure 8 and 9 showing heavier precipitation in future period compared to baseline period.

After the results were obtained for each models and RCPs, the indices as defined for each climate corner (section 3.2.2) were averaged and final score (5-1) was determined with highest ranking (5) assigned for largest increase in indices and one for the lowest. Three RCMs with highest ranks were selected for each climate corner and each RCP, and further processed in final step of selecting RCMs based on comparison of probability density function between historical observation and model simulation for the same period. Similar to initial selection of RCMs based on climatic means, three RCMs were selected out of five for inclusion of more number of RCMs such that climatic variability simulated by each RCMs can be further analyzed.

Figure 16 Percentual change of a. CDD b. CSDI c. WSDI d. R99PTOT between 1976-2005 and 2071-2100

4.1.3. Final selection of RCMs based on past performance

As the scores were averaged for the study area, the resulting scores are shown in Figure 17& Figure 18. Figure 17 shows that ACCESS1-0 has the higher ability to simulate historical climate with significant overlap over observed datasets (0.75). Except for ICHEC-EC-EARTH, all the models generate a skill score greater than 0.6, which indicates that the models performed relatively well.

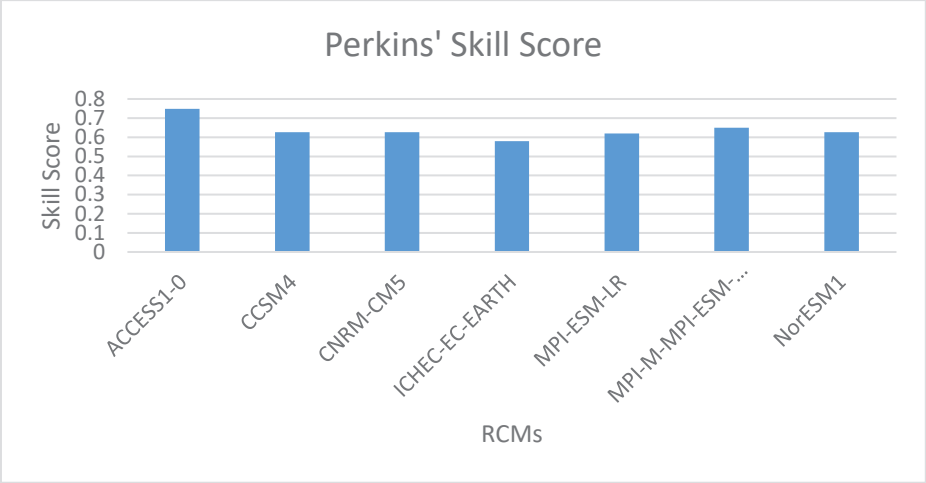

Figure 17 Perkins' Skill Score

Different skill factors based on E. Sanchez et al., 2009 was computed and shown in Figure 18. RCMs driven by GCMs from CSIRO showed similar pattern in context of all skill factors. ICHEC-EC-EARTH seems to perform better in context of all skill factors showing close resemblance to APHRODITE in terms of mean, total area, smaller and higher precipitation amounts and shape of distribution through variance.

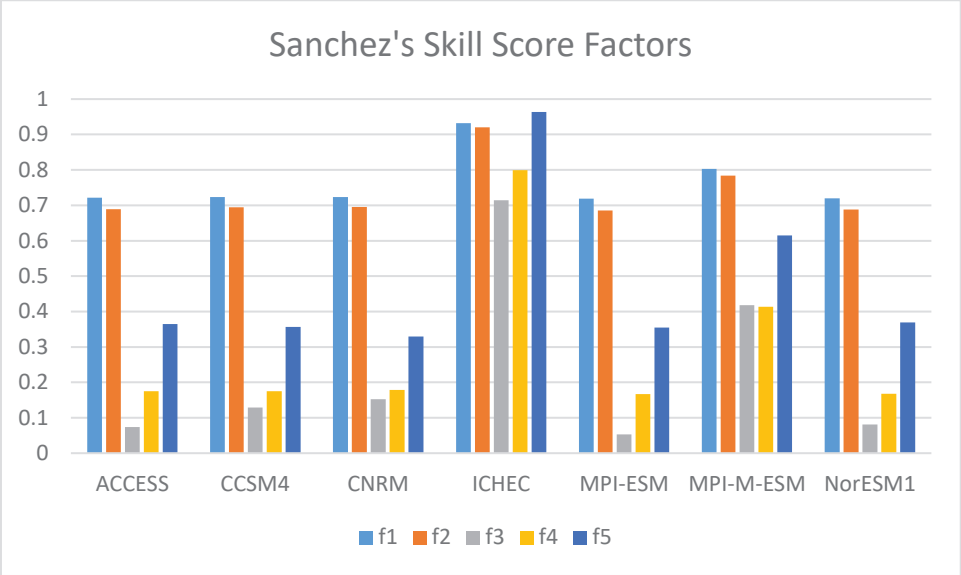

Figure 18 Sanchez Skill Score Factors

Results of final single-weight was computed for each RCM and averaged with Perkins' skill score to obtain the final score for each RCM Table 5.

Table 5Scores for Perkins and Sanchez based RCMs

	ACCESS 1-0	CCSM4	CNRM-CM5	ICHEC-EC-EARTH	MPI-ESM-LR	MPI-M-MPI-ESM-LR	NorESM1
f1	0.72138	0.723528	0.72292	0.931621	0.718989	0.802473	0.719322

f2	0.689169	0.694426	0.695176	0.91986	0.685716	0.783942	0.687742
f3	0.073516	0.129034	0.152007	0.714645	0.052637	0.417926	0.081149
f4	0.174812	0.175062	0.178926	0.798912	0.167278	0.41377	0.168176
f5	0.364668	0.356812	0.329398	0.964068	0.354809	0.615371	0.368818
f	0.00233	0.00405	0.004502	0.471692	0.00154	0.066944	0.00249
Perkins	0.748	0.627	0.626	0.579	0.62	0.65	0.626
FinalScore	0.375165	0.315525	0.315251	0.525428	0.31077	0.358472	0.314245

4.1.4. Monthly temperature and precipitation distribution over Nepal

Figure 19 shows monthly temperature distribution over Nepal resulting from spatially averaged daily temperature data from different RCMs and APHRODITE. All the models seem to fail to capture monthly patterns of temperature, although RCMs driven by GCMs from CSIRO seem to fit well in the months February, March and April. In remaining months, all the RCMs underestimated the monthly temperature values. ICHEC-EC-EARTH and MPI-M-MPI-ESM-LR failed to capture magnitude compared to other RCMs and APHRODITE. Ensemble mean was computed through arithmetic averaging of all RCMs, and it does not show any improvement in capturing monthly temperature distribution over Nepal.

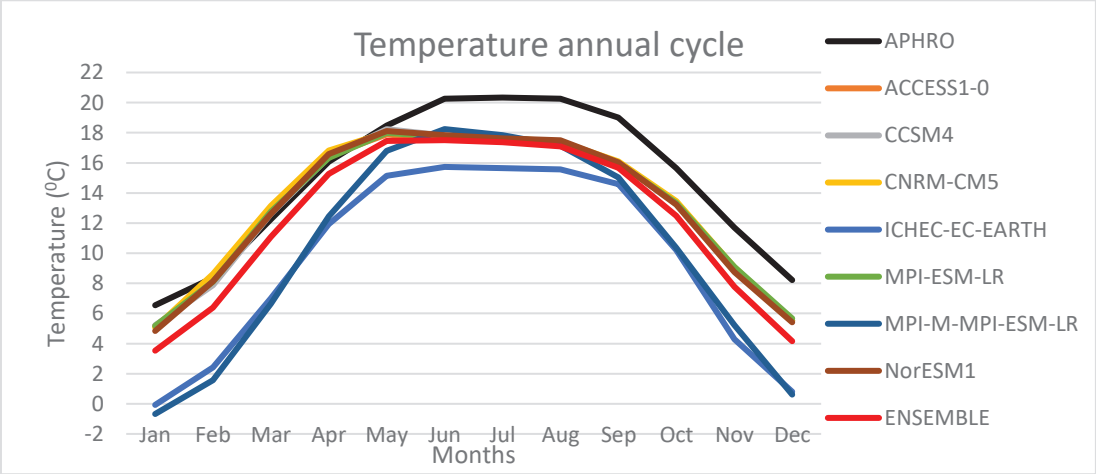

Figure 19 Temperature annual cycle over Nepal

Monthly rainfall distribution over Nepal resulting from spatially averaged daily rainfall data from different RCMs and APHRODITE is shown in Figure 20. RCMs seem to capture the monthly rainfall patterns especially with the highest rainfall occurring month July. Except for ICHEC-EC-EARTH, all the RCMs overestimated precipitation compared to APHRODITE. ICHEC-EC-EARTH was capable to simulate almost the similar amount of precipitation except for the months June, November and December. CNRM-CM5 was found to be performing poorest among all in capturing monthly rainfall amount, highest rainfall amount and overall pattern. As it is clear from Figure 12, almost all RCMs overestimated precipitation in all months, ensemble mean also resulted in poor representation of annual cycle and magnitude compared to APHRODITE.

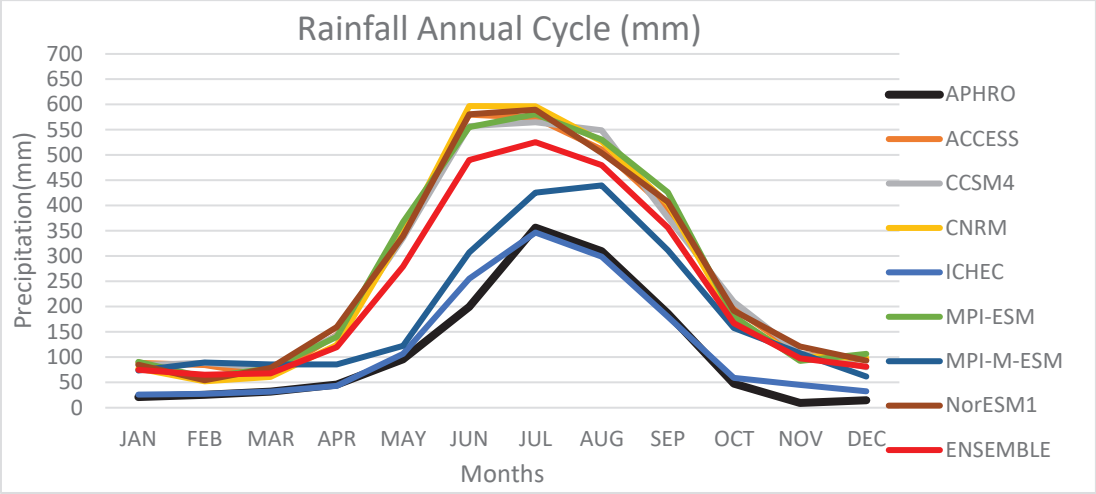

Figure 20 Rainfall annual cycle over Nepal

4.2. Bias Correction

Bias-correction of temperature and precipitation variables for all RCMs selected from section 3.3 was performed. *Figure 21* shows the combined cumulative distribution functions of temperature for APHRODITE, RCM simulated raw historical and future period, and bias-adjusted future period. RCM simulated historical temperature values shows the higher cumulative probability compared to APHRODITE, which explains the under-estimation of temperature by RCMs. In case of future RCM simulated values, each RCM shows different projections. For ACCESS1-0, temperature values are under-estimated, and similar results are found in ICHEC-EC-EARTH RCP4.5. For remaining models, temperature values are over-estimated, which are highest for CCSM4 and CNRM-CM5. The bias- adjusted temperature results are shown by green colored line. Earlier results from inter-comparison of performance of different RCMs from section 5.2 showed the cooling trends for different RCMs, which is also clear from the figure. After bias-correction, these values seems to be corrected.

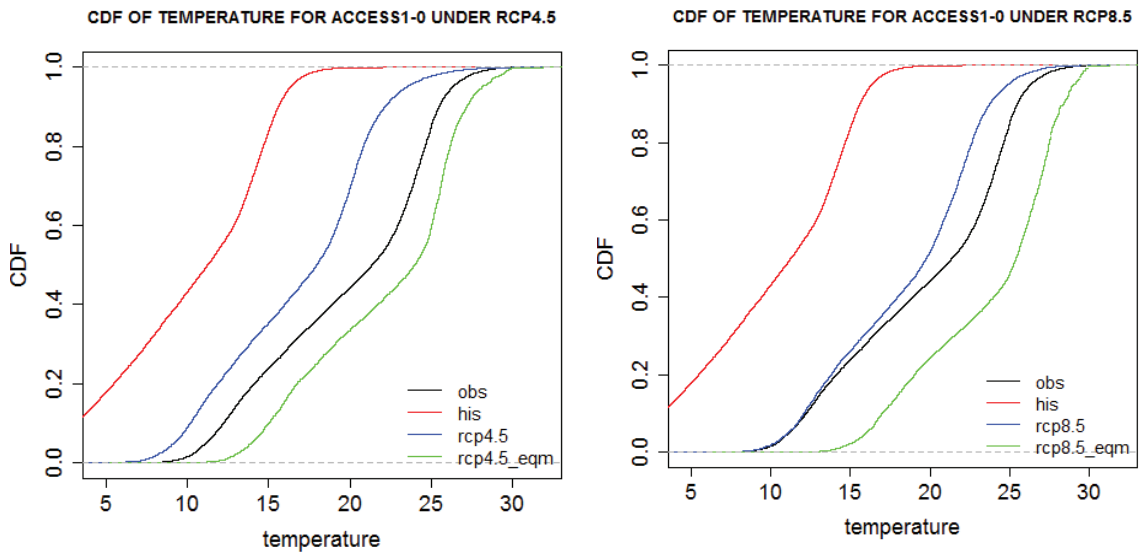

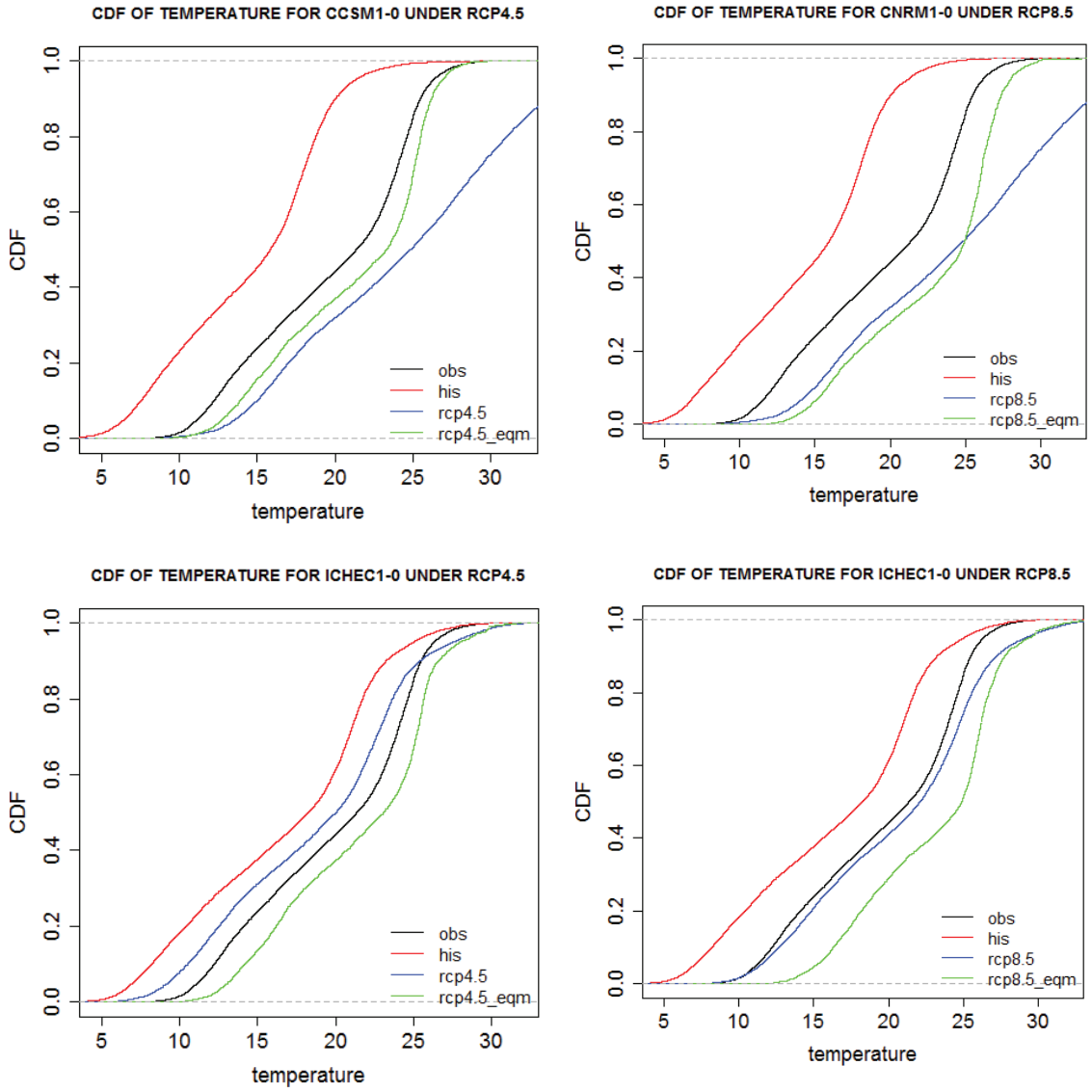

Figure 21 Observed, historical, raw and bias-adjusted CDFs for temperature for different RCMs and RCPs

Similarly, bias- adjusted precipitation values were obtained as shown in **Error! Reference source not found.**. RCM simulated historical precipitation values were found to be over-estimated compared to observation dataset APHRODITE, and it is highly variable with different intensity of precipitation. For lower values of precipitation, RCM estimations donot vary much, however, for higher precipitation amounts, it varies greatly, with highest for CCSM4 and CNRM-CM5. Similar to temperature, bias-adjusted values of precipitation are shown by green line for respective RCMs and RCPs in the figure.

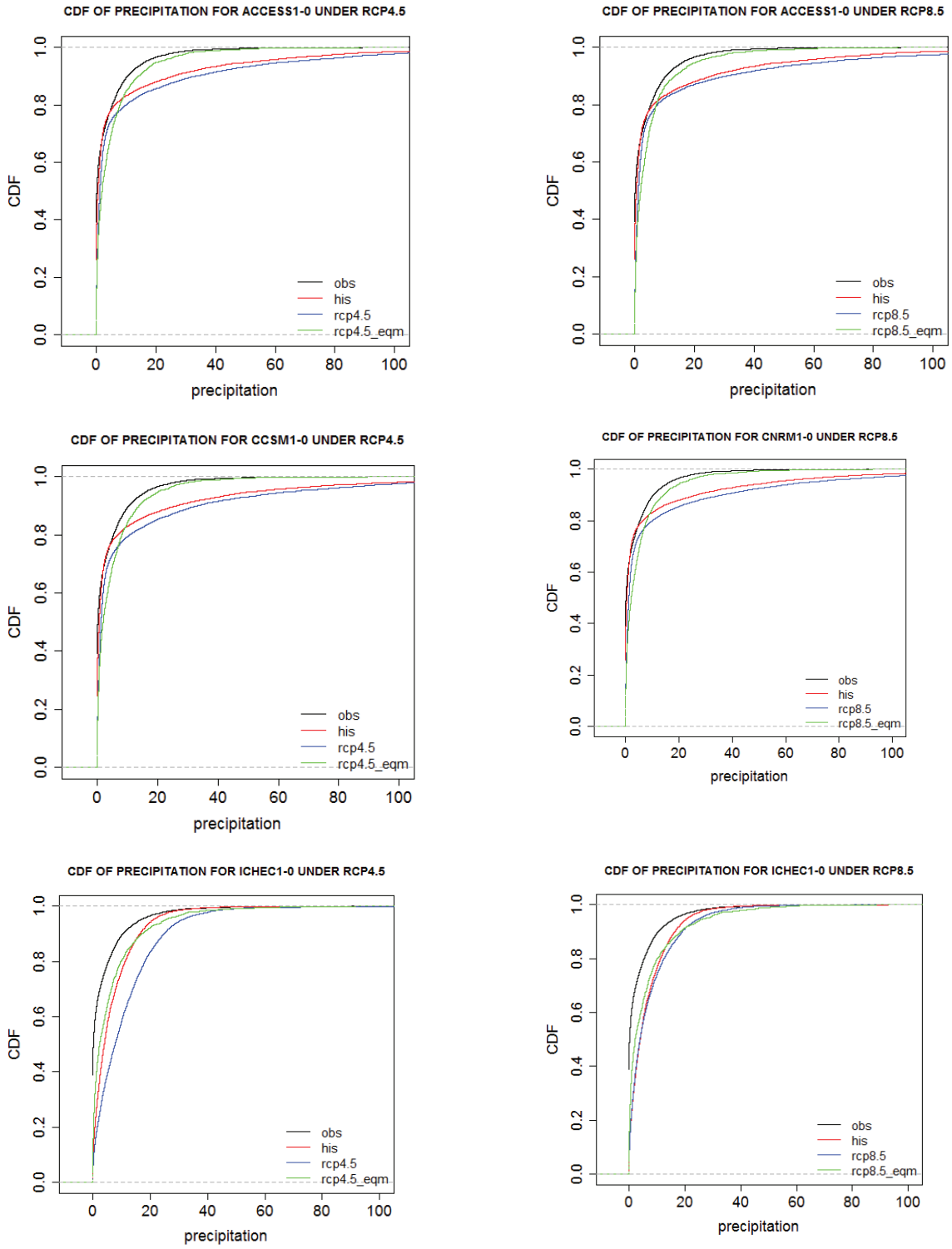

Figure 22 Observed, historical, raw and bias-adjusted CDFs for precipitation for different RCMs and RCPs

4.3. Uncertainty in climate projections

After bias correction, RCM simulated future projections were further evaluated to measure the change in reference to baseline period.

4.3.1. Temperature

Mean monthly temperature for each RCMs selected for RCP 4.5 and RCP 8.5 from section 4.1.3 were plotted against mean monthly temperature during baseline period obtained from APHRODIT dataset, and shown in Figure 23 and **Error! Reference source not found.** respectively. Annual average temperature during baseline period (1976-2005) was about 21.2 ^{0}C, while it ranges from 22.6 ^{0}C for CCSM4 (RCP4.5) to 25.11 ^{0}C for ACCESS1-0 (RCP 8.5). For RCP 4.5, it is likely that the temperature may increase from 1.3 ^{0}C (CCSM4) to 2.3 ^{0}C (ACCESS1-0). Similarly, increment of temperature is more severe for RCP 8.5 which ranges from 3 ^{0}C (CNRM) to 3.8 ^{0}C (ACCESS1-0). Moreover, maximum increment of temperature is likely in February and March, and minimum increment is found in June.

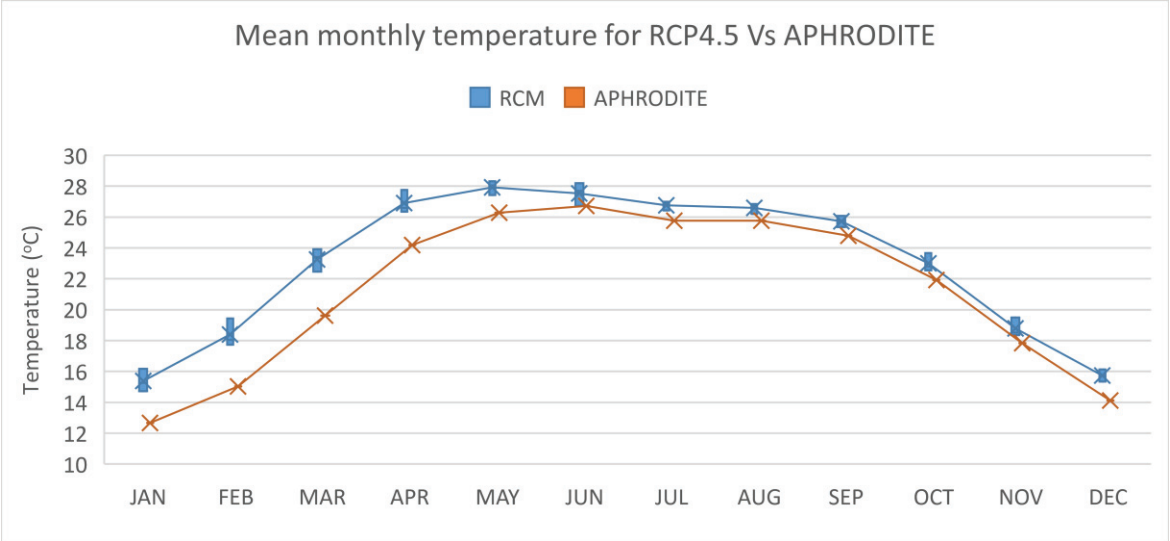

Figure 23 Mean monthly temperature for RCP4.5 Vs APHRODITE

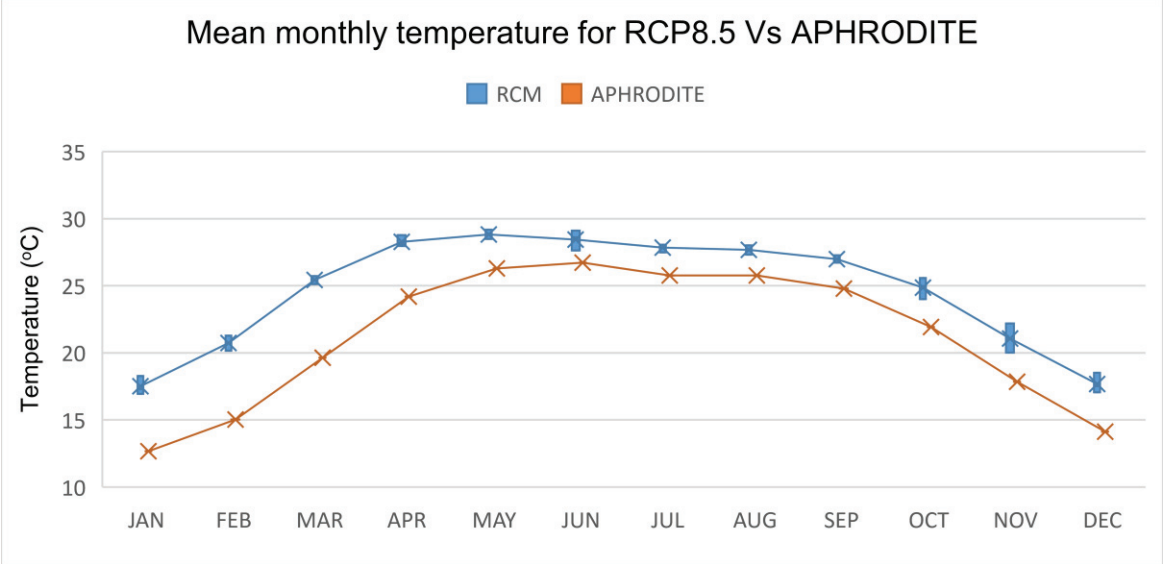

Figure 24 Mean monthly temperature for RCP8.5 Vs APHRODITE

4.3.2. Precipitation

Mean monthly values of precipitation after bias correction of RCM outputs is plotted against APHRODITE dataset for RCP 4.5 and RCP 8.5 in Figure 25 and Figure 26 respectively. Annual average precipitation during baseline period was about 1344 mm, and in future simulation, it ranges from 1453 mm (ICHEC-EC-EARTH, RCP 4.5) to 3011 mm (CCSM4, RCP 8.5). Maximum amount of precipitation is indicated in July, however, only ICHEC-EC-EARTH for RCP 8.5 has higher precipitation compared to APHRODITE. Remaining RCMs predict lower precipitation for July. Minimum precipitation events are found in January, February and March.

For RCP 4.5, increment in annual average precipitation ranges from 109 mm (ICHEC-EC-EARTH) to 414 mm (ACCESS1-0), while for RCP 8.5, it ranges from 337 mm (ICHEC-EC-EARTH) to 483 mm (ACCESS1-0).

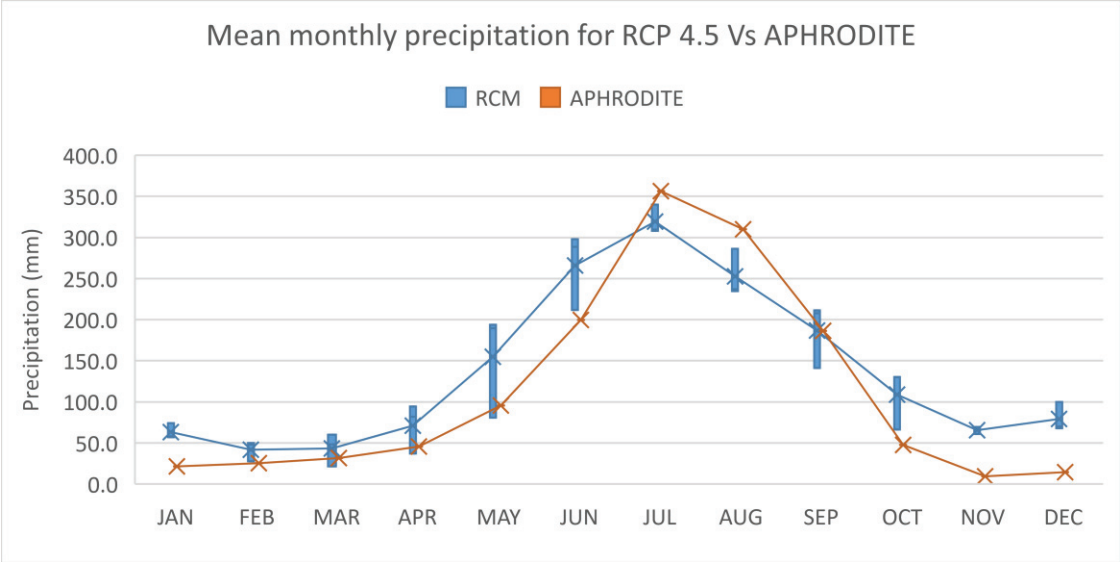

Figure 25 Mean monthly precipitation for RCP 4.5 Vs APHRODITE

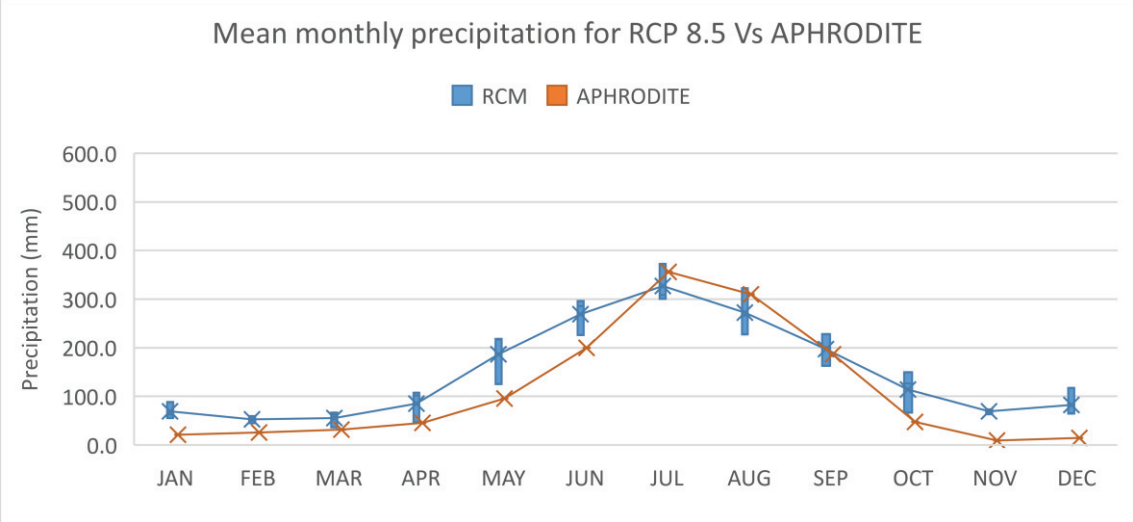

Figure 26 Mean monthly precipitation for RCP 8.5 Vs APHRODITE

4.4. Calibration and validation results of HBV model

The standard version of HBV light model with application of threshold parameter of soil upper zone and recession coefficients was set up with warming period starting from January 1st, 1982. Although the data was available from 1964 for Jalkundi station on daily time scale, period from 1982 to 2005 was used for this study purpose. Calibration of the model involved the period 1983 to 1996, and for validation of the HBV light model, period 1997 to 2005 was chosen. Longer period of years for calibration and validation was considered to optimize the parameters, such that the future flows can be well presented. Results of calibration with objective function include Nash Sutcliffe Efficiency (NSE) to evaluate the overall performance of the model comparing daily simulated values of discharge with observed values for the same period (equation 23). Nash

Sutcliffe Efficiency with logarithmic values (LNSE) were adapted for low flow to reduce the problem of squared difference and the resulting sensitivity to extreme values (equation 24). Logarithmic transformation is helpful in flattening the peaks while low flows are kept the same, thus resulting into increase in influence or sensitivity of low flow values (Krause & Boyle, 2005). Similarly adapted version of Nash Sutcliffe efficiency for high flows (HNSE) was used to evaluate the ability of HBV light model in reproducing high flows (equation 25).

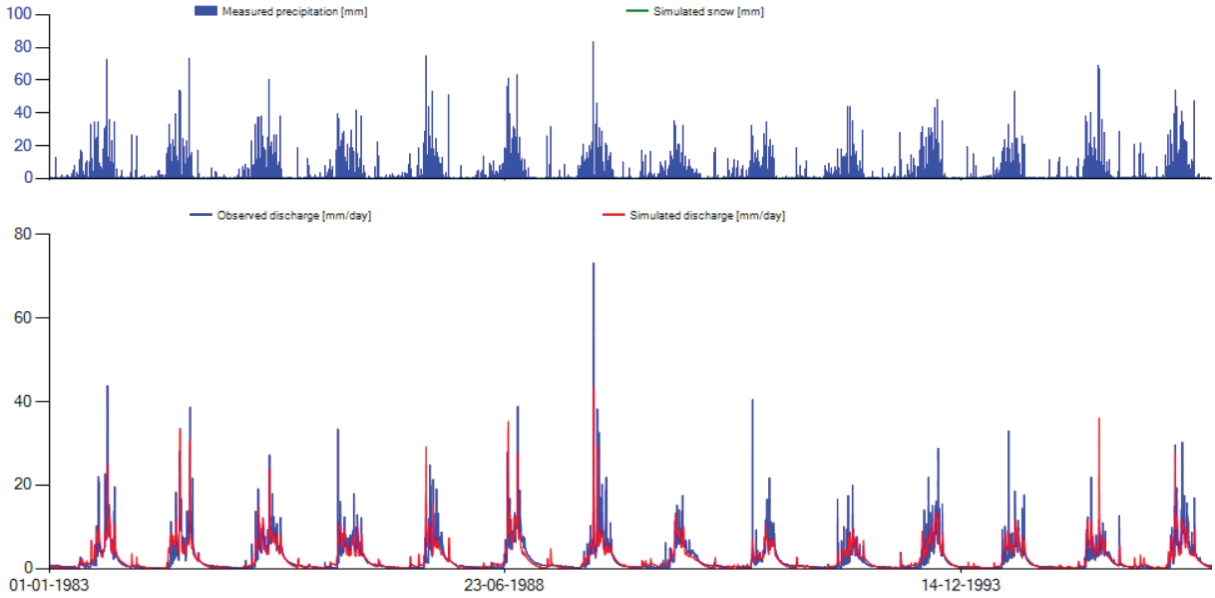

Figure 27 Results of calibrating HBV light model for period 1983-1996

Results of calibrating the model with observed precipitation and discharges including simulated values of discharge for the period 1983-1996 is shown in Figure 27. It shows that the model is capable to simulate low flow well, while high flows are under-estimated throughout the period of calibration. The difference between daily observed and simulated values of stream flow discharge was analyzed and found that the average difference is about 0.91 mm/day, and the maximum and minimum values of differences are zero and as high as 35.44 mm/day. Such highest difference was simulated for 1989-07-15 with precipitation records for last two days were respectively 42.9, 83.6 and 35.2 mm. NSE, LNSE and HNSE for the calibration period are 0.71, 0.76 and -0.18 respectively. Thus the performance of the model can be concluded as good, however the results for peak flows are subject to further optimization of the model parameters.

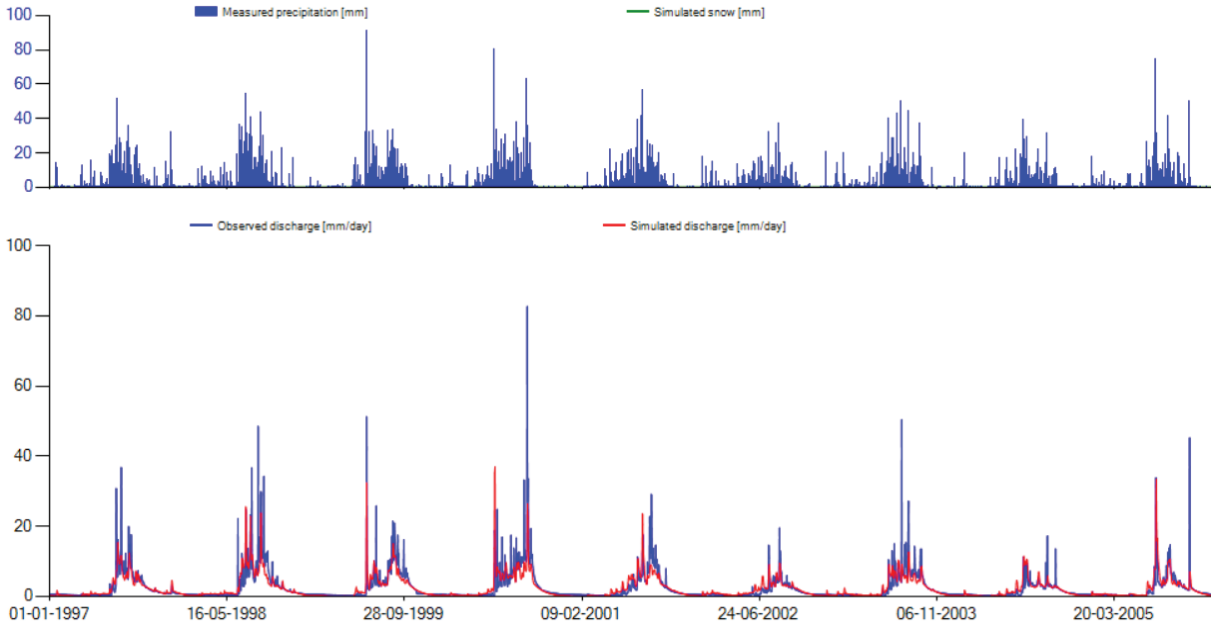

Figure 28 Results of validating HBV light model for period 1997-2005

Results of validating the model with the same optimized sets of parameters used during calibration of the model is shown in Figure 28. It shows that the model is capable enough to simulate the low flow and overall pattern of seasonal flows for the validation period of 1997-2005, however, high flows are under-estimated. Mean difference between simulated and observed values of discharge is 0.96 mm per day, with values ranging from 64.7 mm/day to 0.001 mm/day. NSE, LNSE and HNSE are 0.61, infinity, -0.59 respectively. With NSE values of 0.61, the model has only satisfactory performance.

4.5. Simulation of future flow (2071-2100)

4.5.1. Simulation of future flows without bias correction of RCM data

The optimized parameter set during calibration of HBV light model was used to simulate future stream flow discharges. Daily potential evapo-transpiration was calculated based on future data of temperature from each RCM and each RCP. Thus obtained PET values were averaged to obtain mean monthly PET for each RCMs, and fed into hydrological model. Mean monthly values of simulated stream flow discharge based on RCMs finalized from section 4.1 were plotted against the discharge values of baseline period as shown in Figure 29. RCP 4.5 is represented by blue coloured lines and RCP 8.5 is represented by green lines. Seasonal shift in stream flow discharge is clearly visible as the observed values of discharge for baseline period has August as the maximum discharge while the most of the RCMs show July. This is also clear from Figure 9 where largest absolute change of precipitation amount for all RCMs and RCPs are shown in July compared to August. Except for ICHEC-EC-EARTH, all RCMs show overall increase in discharge in future for all months. Low flow months (November, December and January) also have higher flows compared to baseline period. This is also evidence from Figures 9, 10 and 11 which show increase in precipitation events. ICHEC-EC-EARTH shows decrease in monthly discharge values for months August, September and October. Discharge values range from as low as 22.2 cubic meter

per second for CNRM-CM5 for RCP 8.5 in March to 1491 cubic meter per second for ACCESS1-0 for RCP 8.5 in July.

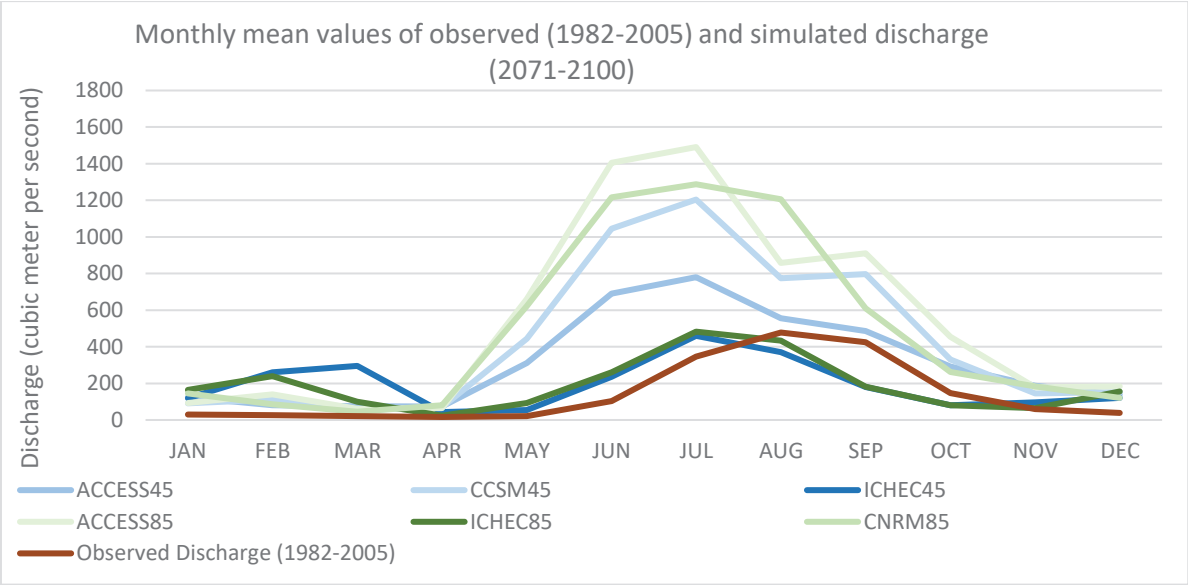

Figure 29 Monthly mean values of observed (1982-2005) and simulated stream flow discharge (2071-2100)

Similarly, Figure 30 indicates absolute change in mean monthly discharge values between baseline and future period for each RCMs and RCPs. Decline of stream flow discharge is shown by ICHEC-EC-EARTH for August, September and October with lowest values for RCP 4.5 (245.3 cubic meter per second) in September. Remaining RCMs show positive change for all months with least positive change during April, and highest for June. However, ICHEC-EC-EARTH shows highest positive change for February and March.

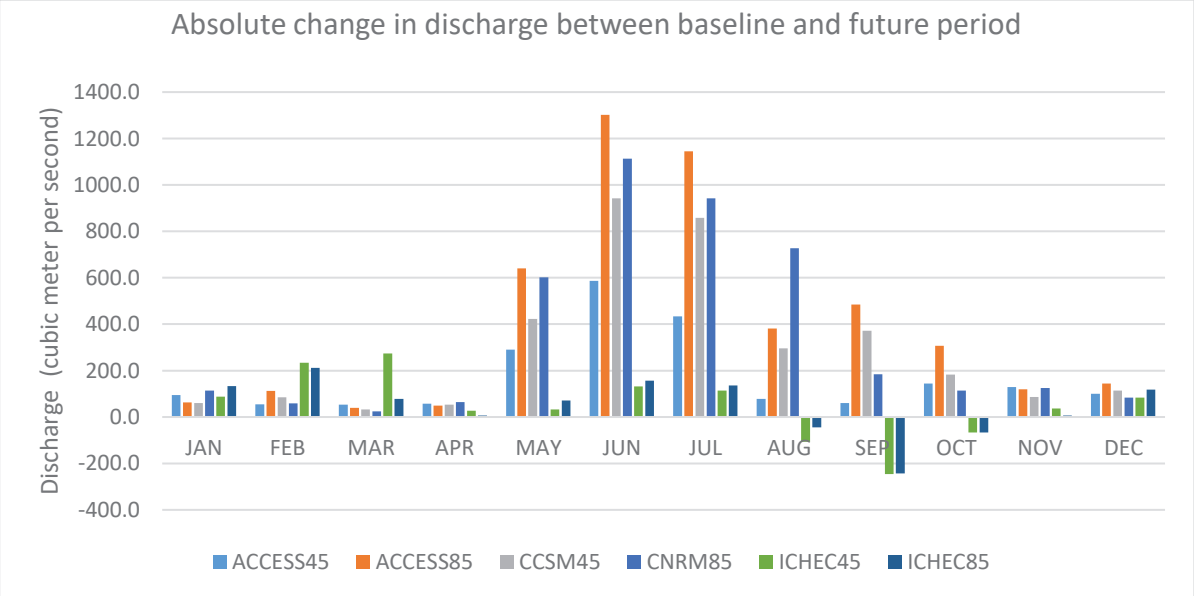

Figure 30 Absolute change in discharge between baseline and future period

4.5.2. Simulation of future flows with bias correction

RCMs selected from section 4.1 were bias corrected applying empirical quantile mapping for temperature and precipitation values at daily time scale. Thus, bias corrected temperature and precipitation values were fed into HBV model along with monthly average values of PET, computed with bias corrected temperature data. Finally, the optimized parameter set used earlier during calibration of HBV light model for baseline period was used to simulate future flows. Figure 31 shows the monthly average discharge for each RCMs after bias correction. Figure 32 indicates monthly average discharge values for each RCMs with and without bias correction, along with observed values for historical period. The overall shift in seasonal pattern of maximum discharge is visible for all RCMs. It further means that the bias correction technique preserves the seasonal pattern. However, there is large shift in magnitude of discharge values after bias correction. Figure 32 gives the difference in simulated discharge values after bias correction.

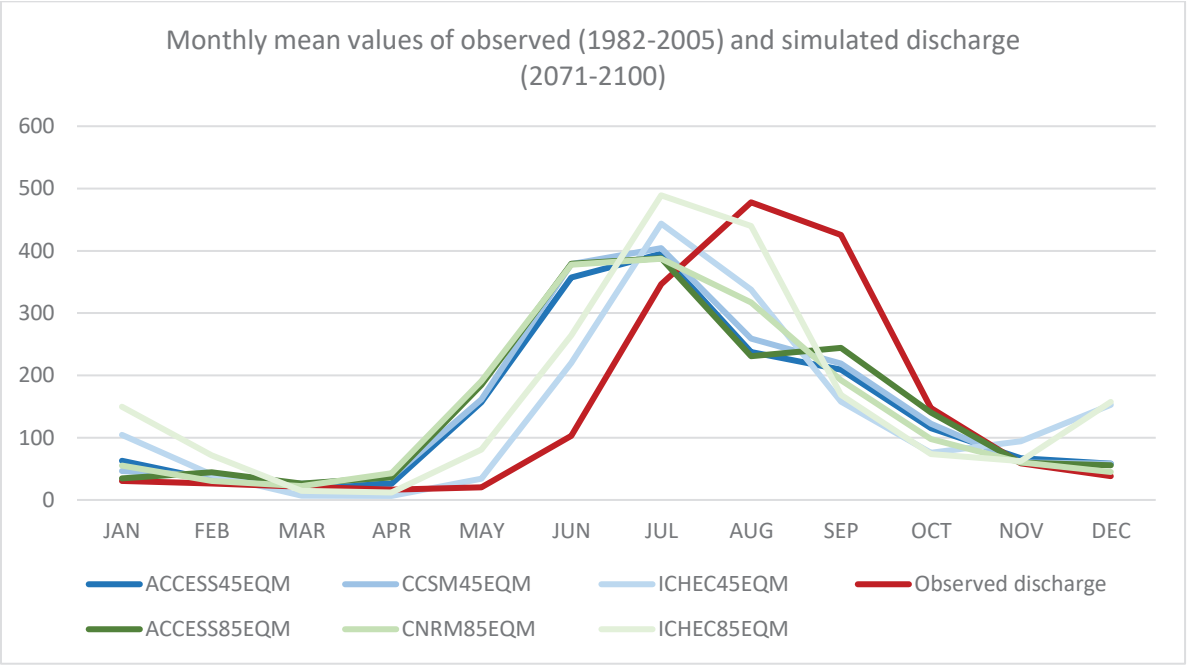

Figure 31 Monthly mean values of observed (1982-2005), and simulated discharge (2071-2100) after bias correction

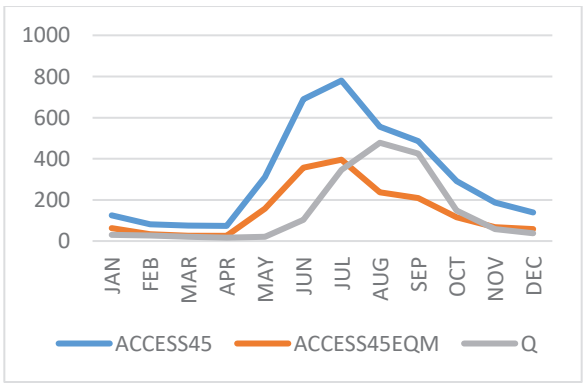

(a)

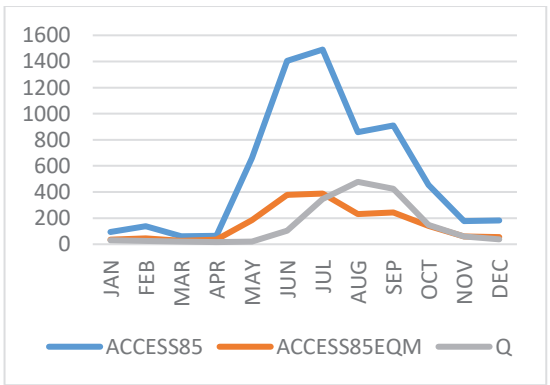

(b)

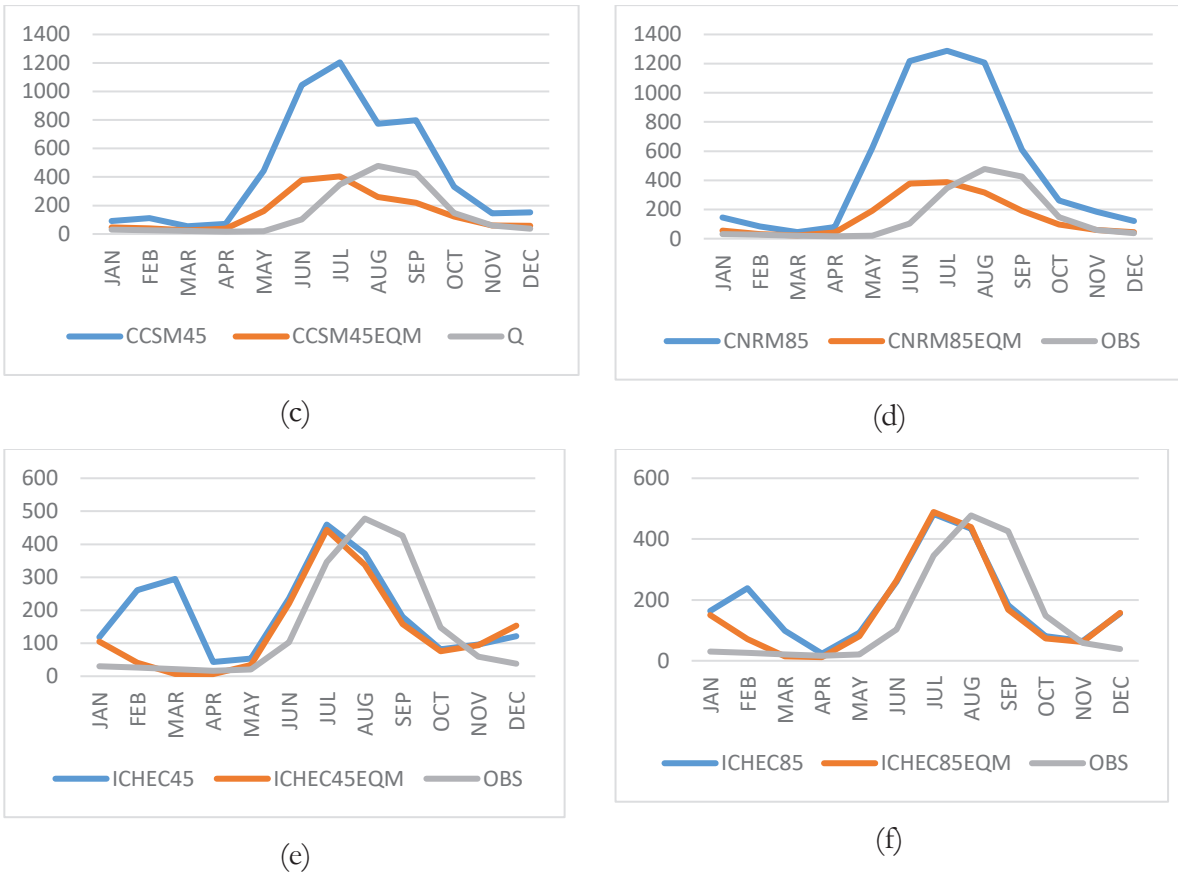

Figure 32 Monthly discharge for baseline period, and future period with and without bias correction for each RCMs

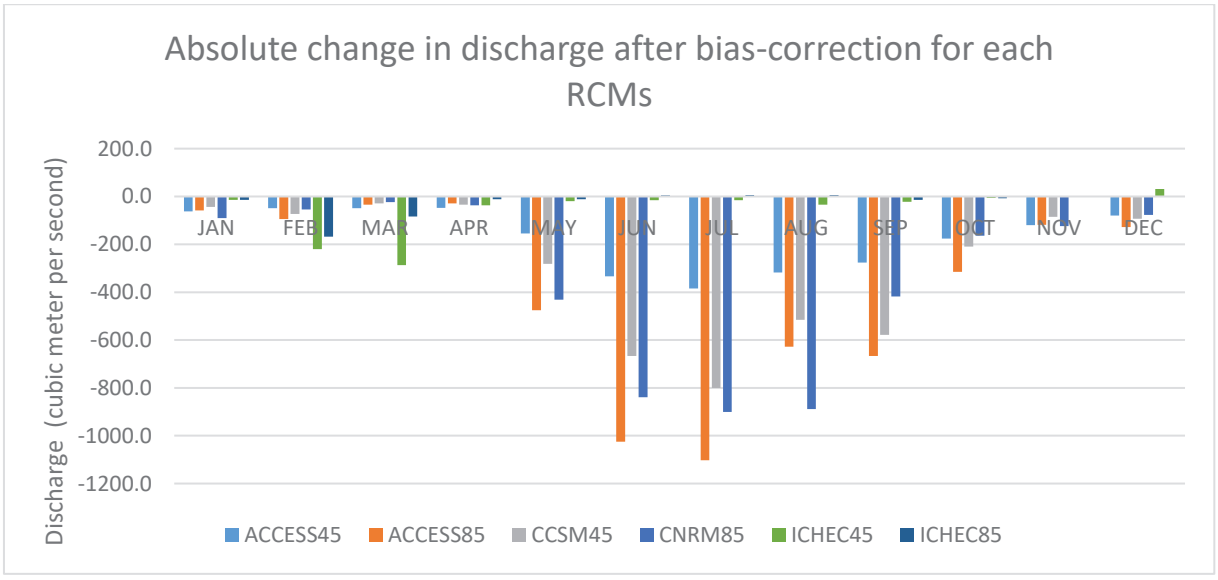

Figure 33 Absolute change in discharge after bias-correction for each RCMs

Results of bias correction are highest for ACCESS 1-0 for RCP 8.5 as shown in Figure 33, with lowest change for ICHEC-EC-EARTH. May, June, July, August, and September have higher

adjustment of raw simulated RCM based discharge compared to other months. Increase in discharge values after bias correction is only seen in ICHEC-EC-EARTH by about 6 cubic meter per second for RCP 8.5 in July while ACCESS1-0 for RCP 8.5 shows the steepest decline in discharge values (-1102 cubic meter per second). Simulated values of discharge after bias correction of RCM data for future period are closer with the observed values of baseline period. These results can be interpreted from Figure 22, which shows the results of bias-correction of precipitation for each RCMs. Figure 31 and Table 6 give range of projections of monthly mean values of discharge, and also represent uncertainties in RCMs based future discharges in West Rapti.

Table 6 Annual average, and monthly maximum and minimum discharge values for each RCMs after bias correction including for observed period

Climate Corner	RCP	RCMs	AVG	MAX	MIN
		OBSERVED	142.7185	477.8151	16.49207
COLD,DRY & WARM,DRY	RCP 4.5	ACCESS 1-0	145.3359	395.3973	25.87788
COLD,WET	RCP 4.5	CCSM4	150.8423	404.2724	25.39176
WARM,WET	RCP 4.5	ICHEC-EC-EARTH	139.5987	443.6699	6.432238
WARM, DRY	RCP 8.5	ACCESS 1-0	151.995	388.0804	26.24359
COLD,DRY & COLD,WET	RCP 8.5	CNRM	151.5497	387.2095	22.20457
WARM,WET	RCP 8.5	ICHEC-EC-EARTH	165.2763	489.0239	11.95725

4.6. Analysis of extreme flows

Extreme low flows and high flows were defined for values less than 10th percentile and values greater than 90th percentile respectively as explained in section 3.2. Results from bias-corrected RCMs only are considered for extreme flow analysis here. Maximum and minimum values of historical data on discharge were calculated, and difference of maximum value and 90th percentile was considered to define bin size, and number of bins for evaluating frequency distribution of extreme low flows. Similar approach was followed for analysing frequency distribution of extreme high flows by considering difference of 90th percentile and maximum flow.

Histogram of daily discharge under extreme low flow condition based on RCMs for RCP 4.5 is shown in Figure 34. Observed discharge from station Jalkundi is also plotted for comparison. The lowest discharge as seen from the histogram is around 2 cubic meter per second, however the future projections by RCMs under RCP 4.5 shows larger number of events with zero flow condition. In this case, ICHEC-EC-EARTH indicates higher tendency towards no flow condition. However, flows from 2 – 11 cubic meter per second point towards increase in low flow conditions compared to historical period. This is also evident from Figure 25 which shows the higher amount of monthly mean precipitation for RCP 4.5 in the dry season (March and April) in future period (ensemble mean of RCMs) compared to historical period. Yet, the flows ranging 13-14 cubic meter per second indicate decrease in future period. First quartiles during dry season as shown in Figure 25 also show lower values of precipitation from RCMs compared to observed precipitation. Based

on histogram, ICHEC-EC-EARTH shows the largest variability in discharge while ACCESS1-0 and CCSM4 show similar pattern of frequencies for extreme low flows.

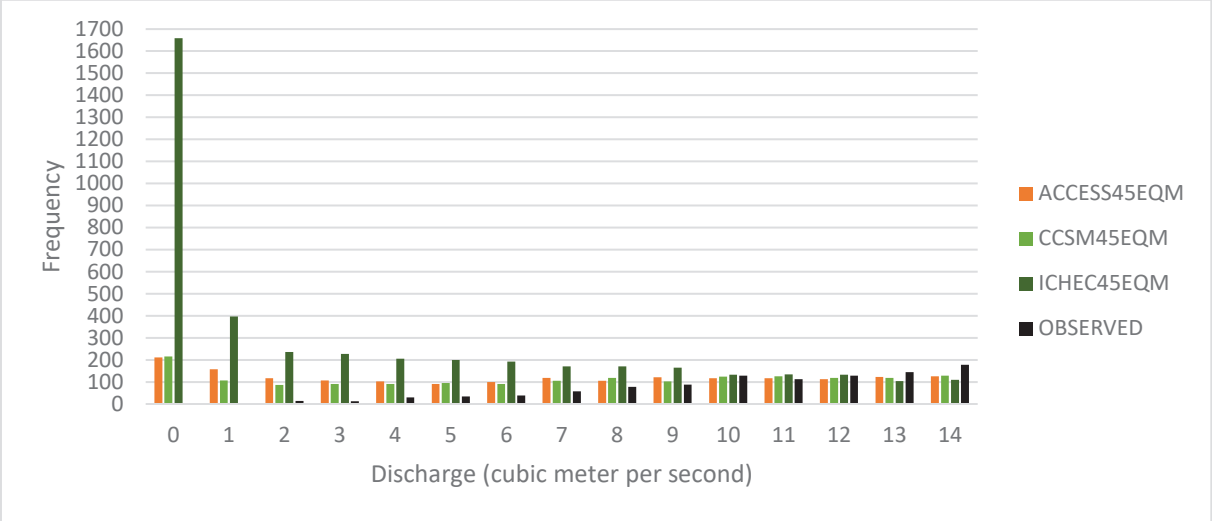

Figure 34 Frequency of daily stream flow discharge of extreme low flows for RCP4.5

Similarly, Figure 35 shows the frequency distribution of extreme low flows for RCP 8.5. The number of events for each bin is lower compared to RCP 4.5. For lower values of discharge (2-9 cubic meter per second), there is higher frequency of events under RCP 8.5. For discharge values ranging from 11 – 14 cubic meter per second, RCMs indicate towards drier condition. These results are also evident from Figure 26 which indicates overall increase in precipitation from ensemble mean of RCMs.

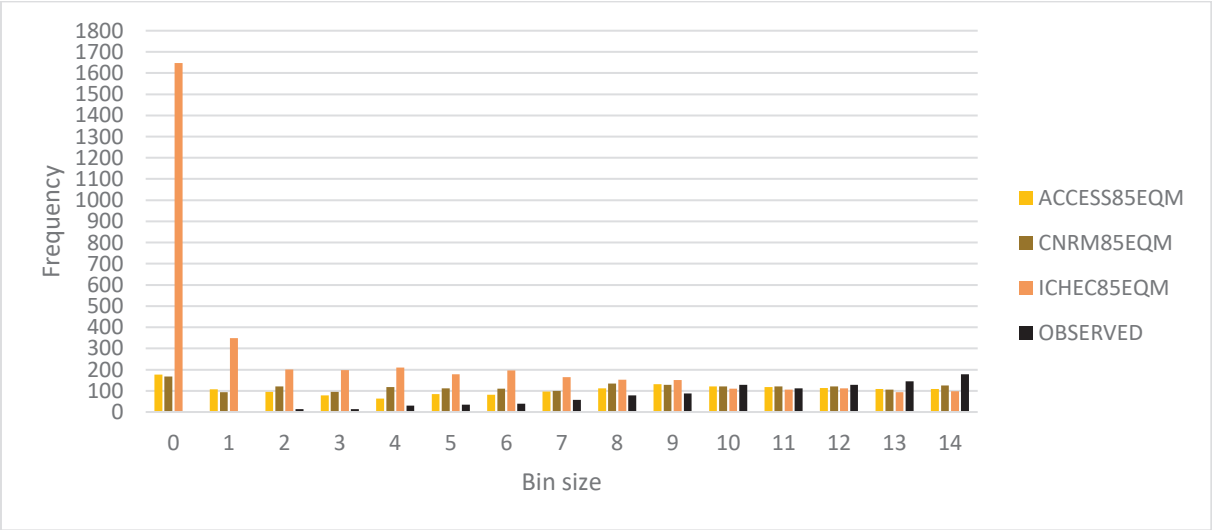

Figure 35 Frequency of daily stream flow discharge of extreme low flows for RCP 8.5

Histogram of daily discharge for extreme high flows ranging from 490 to 2190 cubic meter per seconds for all RCMs under RCP 4.5 along with observation data is shown in Figure 36. Maximum value of observed- historical discharge is 7196 cubic meter per second, however in future simulation, it extends from 2276 – 36008 cubic meter per second. Hence, it was not possible to display the whole series of histogram here. The figure clearly shows that for discharge values

ranging from 490-590 cubic meter per second, frequency of occurrence is larger in observed dataset compared to RCM simulations. However, the occurrence of high flow over the 990 cubic meter per second is more frequent in RCM simulations than historical observations. ICHEC-EC-EARTH seems to predict higher frequency of extreme events compared to other RCMs for discharge values greater than 990 cubic meter per second. These extreme high flows normally occur in monsoon season extending from June till September. Precipitation results from Figure 25 also indicate towards higher precipitation events in July and August compared to historical observations, which could be the possible reason for such highly extreme flows in future.

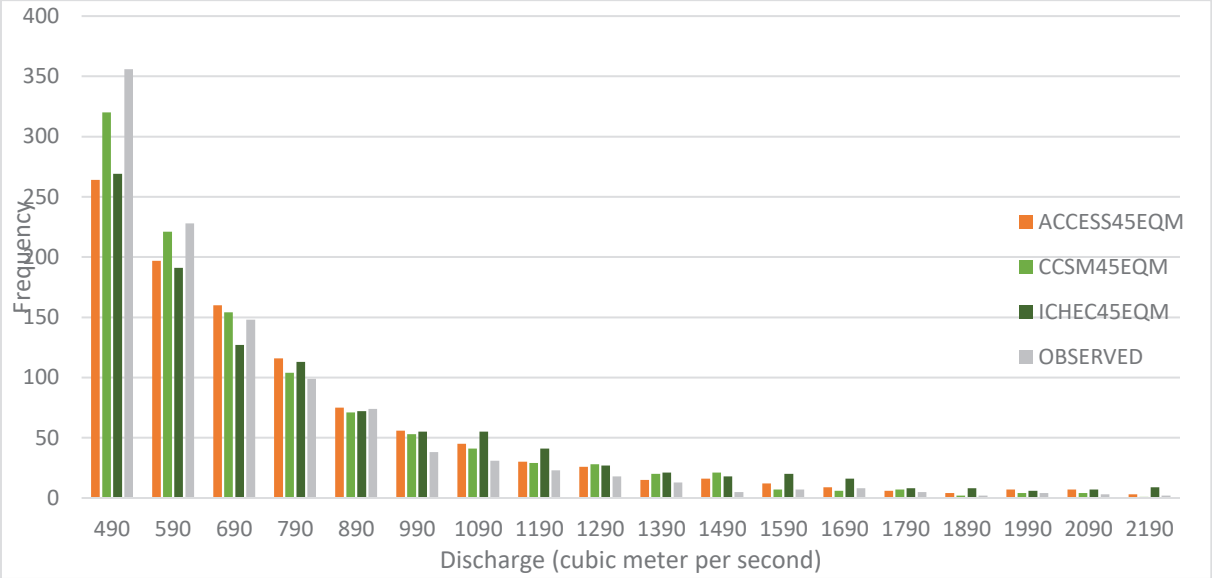

Figure 36 Frequency of daily stream flow discharge of extreme high flows for RCP4.5

Similarly frequency distribution of extreme high flows under RCP 8.5 is shown in Figure 37. The frequency of occurrence of discharge from 490 to 690 cubic meter per second is higher in observation dataset compared to RCM simulation. For all RCMs, frequency of occurrence of high flows above 990 cubic meter per second is higher compared to RCP 4.5.

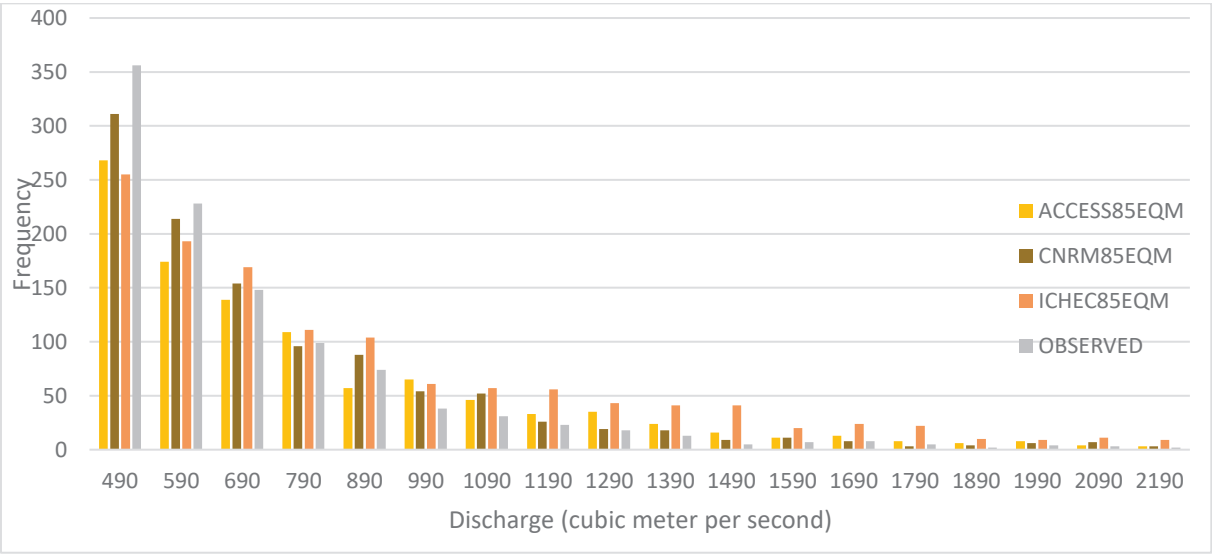

Figure 37 Frequency of daily stream flow discharge of extreme high flows for RCP8.5

5. DISCUSSION

5.1. Selection of regional climate models

Assessment of regional climate change requires ensemble simulations by different global and regional climate model combinations, and experiments in CORDEX South Asia follows the same approach which further helps to interpret the spread of simulated results (Figure 6 and 9) as an outcome of inherent and methodological uncertainties in climate modeling (Teichmann et al., 2013). This study shows that all RCMs have been able to capture the seasonal pattern of annual cycle of monthly temperature (Figure 19), although values are overestimated. In Figure 20, it is shown that temporal precipitation variability at monthly time step is overestimated by most models, except for the ICHEC-EC-EARTH.

Previous studies have shown that winter temperatures are increasing faster than summer temperatures (Figure 6) while the winter precipitation does not show any significant trend. Compared to summer months, winter is expected to be drier (Figure 9) (Charles, Chiew, & Zheng, 2016). Figure 6 and Figure 7 show that mean values of absolute changes in temperature is higher than median, and it indicates that relative dispersion of middle 50 percent of ΔT is towards minimum values. The results are similar to scatterplots in Figure 12 and Figure 13. Increase of CSDI with associated decrease in WSDI (Figure 16) has been reported by earlier studies, and this could be possibly due to aerosol cooling as aerosols absorb incoming solar radiation, thus reducing surface solar absorption and leading to land cooling (Sanap, Pandithurai, & Manoj, 2015).

After a three step sequential selection approach, ACCESS 1-0 (cold, dry & warm, dry), ICHEC-EC-EARTH (warm, wet) and CCSM4 (cold, wet) were selected for RCP 4,5. Similarly, CNRM-CM5 (cold, dry), ICHEC-EC-EARTH (warm, wet), CNRM-CM5 (cold, wet) and ACCESS1-0 (warm, dry) were selected for RCP 8.5.

This study adopted the evaluation of climatic means and extreme events from RCM simulated data before comparing the RCMs with observation datasets. In general, climate impact assessment studies are based on an assumption that a more realistic simulation of present-day climate implies more reliable projections of future climate change, however, the higher resolution in RCMs could introduce additional noise at smaller spatial scales, and thus wiping out the climate change signals (Paeth & Mannig, 2012). Feser et al., 2011, on the added value to GCMs data by RCMs, came to conclusion that RCMs can add value, but only for certain variables and locations. Therefore, assessment of uncertainties related to RCMs is important before application of RCMs directly in the study of impacts of climate change in sectors like water resources and agriculture (Syed et al., 2014). This led to selection of RCMs based on range in projected climate change as the first step of filtering RCMs, before evaluating the skills of RCMs to simulate past climate. Besides, RCPs only offer representative scenario of what the future could possibly be like, and it is still an incomplete package of socio-economic conditions, emissions and climate projections (van Vuuren et al., 2011). Moreover, uncertainties in climate projections in earlier studies as discussed in section 3.2 further concludes on the poor skills of existing climate models in simulating precipitation dynamics over the study area. Thus, inclusion of all possible range of projections involving final selection of RCMs based on past performance is very likely to well represent both present and future climate.

The first limitation of this study is related to the scale issue, as the projected changes are averaged over the entire study area in selecting RCMs based on changes in climatic means, which may very likely dilute the spatial variation in projected changes. Similar spatial averaging is applied in the second and third step of selecting RCMs based on changes in climatic extremes and based on past performance respectively. Frequency distribution of precipitation against the corresponding observations and their spatial distribution offer better understanding of ability of RCMs in reproducing spatial variability.

5.2. Uncorrected RCM simulation and bias correction

Figure 19 and Figure 20 shows the underestimation of temperature and overestimation of precipitation respectively, mainly in winter season. Mishra, 2015 has reported similar results from CORDEX South Asia RCMs, and further concluded that overestimation of precipitation could be partially attributed to the fact that most of the observations do not include solid precipitation.

Comparison of Figure 6 with Figure 23 and **Error! Reference source not found.** also suggest a d ecrease in range of projections after bias correction. Climate models show systematic biases in warm and dry climates which result in the regional amplification of global warming (Boberg & Christensen, 2012). Source of larger uncertainty comes from uncorrected RCM simulation (Teutschbein & Seibert, 2012), which explains the necessity of bias correction of climate model output to assure meaningful results in applications like hydrologic and water resources assessment.

Values and evolution of tails of probability density functions define occurrence and frequency of extreme events, which have significant importance in impact modeling. Recent studies on effect of bias-adjustment of climate variables, both in present and future has shown that bias-adjusted PDF (*Figure 21* and *Figure 22)* of extreme events under climate change can differ from the original (non bias-adjusted) estimates, and further concluded on the necessity of bias-adjustment of present and future climates (Dosio, 2016). Ghimire et al., 2015 evaluated 11 CORDEX experiments for their ability to capture and characterize the precipitation climatology over Himalayan region, and reported under-estimation of precipitation by the experiments. Ghimire et al., 2015 reported that systematic biases could lead to over-estimation of frequency of entire range of precipitation, and further suggested on the application of bias correction technique.

The possible reasons for under-estimation was related to the weakness in model physics or error in observation dataset. Another limitation of this study includes the absence of evaluation of APHRODITE dataset with ground stations. Besides, correction of APHRODITE for different elevation was not performed.

5.3. Future climate

Largest increase in temperature and precipitation are observed in winter and spring seasons as shown by Figure 23 to 26. Besides, larger proportion of decrease in monsoon is also revealed from the figures. Studies related to South Asian precipitation has revealed the suppression in monsoon dynamics and summer precipitation due to enhanced GHG emissions which is visible from Figure 25 and Figure 26 (Moetasim Ashfaq et al., 2009; Syed et al., 2014). However, similar studies by Rajbhandari et al., 2016 over Koshi basin of Nepal have come up with increase in rainfall during summer with winter rainfall decreasing by 2050. Yet, larger warming was reported in winter compared to summer, which is also shown by Figure 23 and **Error! Reference source not found.**.

The result of this study shows that increase in winter and spring temperature for all RCMs under RCP 4.5 ranges from 2.84 ^{0}C to 4.39 ^{0}C, and under RCP 8.5, it ranges from 3.9 ^{0}C to 6.24 ^{0}C. Temperature projection for summer under RCP 4.5 ranges from 0.62 ^{0}C to 0.97 ^{0}C, and under RCP 8.5, it ranges from 0.06 ^{0}C to 1.9 ^{0}C.

Similarly, precipitation under RCP 4.5 for winter increases from 2.4 mm to 103 mm compared to observational dataset, while the summer precipitation shows mixed pattern. In July and August, there is decrease in precipitation, and range from -16 mm to -75 mm, however June and September show increase in precipitation ranging from 12 mm to 355 mm. In case of RCP 8.5, the results are similar to RCP 4.5, however ICHEC-EC-EARTH show marked increase in precipitation ranging up to 355 mm compared to historical period. Warmer temperatures increase atmospheric moisture content, overwhelming weakening monsoon circulation (Charles et al., 2016). Rajbhandari et al., 2014 studied projected changes in climate over Indus using PRECIS and found that non-uniform changes in precipitation overall, with greater warming in winter than in other season by the end of this century.

5.4. Future water resources

Figure 32 shows the increment in mean discharge values in July by all RCMs compared historical dataset. However, absolute change of discharge values between baseline and future period indicates that larger increase occur in June. For RCP 4.5, it ranges from 117 cubic meter per second to 275 cubic meter per second, and for RCP 8.5, it ranges from 161 cubic meter per second to 276 cubic meter per second. This is also evident from Figure 25 and Figure 26 which shows the largest shift in precipitation amount in June for both RCPs, and Dams et al., 2015 also has come up with similar results in his study Kleine Nete catchment, Belgium. However, PERERA et al., 2013 studied impact of climate change on flood hazards in lower West Rapti basin using MRI-AGCM outputs and concluded the shifting of high discharge seasons from June/July to September/October for A1B emission scenario.

For RCP 4.5, increment of annual mean values of discharge between baseline and future period ranges from 2.6 cubic meter per second to 8.1 cubic meter per second. ICHEC-EC-EARTH shows the negative signal with decrease of discharge values by 3.1 cubic meter per second. For RCP 8.5, it ranges from 8.8 cubic meter per second to 44.8 cubic per second.

The whole basin was spatially lumped into HBV Light model, which is other limitation of this research. As the spatial features like land cover and land use was spatially aggregated, this could be the reason for not satisfactory results for high flows during calibration and validation. Moreover, altitudinal variation is also not incorporated in temperature and precipitation correction.

6. CONCLUSION

Selection of single RCM as the best fit to represent the climate is a very complex task as all the RCMs deviate much from the observation dataset. Moreover, each RCM is driven by governing GCM with different initial and boundary conditions, which further make it difficult to conclude on the RCM and governing physics behind it. Inherent systematic biases owing to resolution or representation of small-scale forcing and processes in RCMs cannot be neglected.

This study evaluated the performance of seven CORDEX South Asia RCMs in terms of range of projections by all RCMs, their ability to simulate climate variability and extremes, and capture and characterize the temperature and precipitation climatology over the study area for four climate corners. APHRODITE dataset was taken as the observation dataset showed better results in the study area, and also for the fact that vertical interpolation is already incorporated in the dataset. 30 years from 1976 to 2005 was considered as historical or baseline period, and future period was considered from 2071-2100. Similarly discharge data from station Jalkundi was used to calibrate and validate HBV model for period 1982-1996 and 1997-2005 respectively. RCM simulated future projection were bias corrected using empirical quantile mapping technique and further used for estimating future flows, and HBV light model was used for this purpose.

The RCMs show wide variations in simulating precipitation and temperature over the study region indicating uncertainty in climate projections and inability of RCMs to simulate regional climate. Nearly all RCMs underestimated mean annual temperature except for months March and April by CCSM4, CNRM-CM5 and NorESM1. Underestimation of monthly mean temperature ranges from 0.23 ^{0}C to 7.59 ^{0}C. All models except for ICHEC-EC-EARTH and MPI-M-MPI-ESM-LR slight overestimated temperature in March and April by 0.2 – 0.8 ^{0}C. Similarly, for precipitation, all RCMs overestimated mean annual rainfall amounts except for ICHEC-EC-EARTH. It ranges from 0.27 mm (ICHEC-EC-EARTH) for March to 397 mm by CNRM-CM5 in June. ICHEC-EC-EARTH is the only model which under-estimated precipitation in April and July – September by around 9 mm. These variations in historical simulations indicate significant differences between performances of the RCMs. These results explains the necessity of bias correction of climate model output before its application in water resource assessments.

RCMs finalized through three steps sequential-climate model-selection procedure for each climate corners under RCP 4.5 and RCP 8.5 was bias corrected following empirical quantile mapping technique. Thus, an improvement of raw RCM temperature and precipitation series for future climate conditions was achieved. Annual average temperature is expected to rise by 1.4^{0}C to 2.3 ^{0}C for RCP 4.5, and by 3 ^{0}C to 3.9 ^{0}C for RCP 8.5 by the end of century. Similarly, annual average precipitation is likely to increase by 109 mm to 414 mm for RCP 4.5, and by 337 mm to 488 mm for RCP 8.5 in future period.

Based on bias-corrected projections, temporal shift of peak runoff generation from August to July was observed. However, overall decrease in mean monthly stream flows during monsoon is observed while increase in low flows is indicated for both RCPs. For RCP 4.5, increment of annual mean values of discharge between baseline and future period ranges from 2.6 cubic meter per second to 8.1 cubic meter per second. ICHEC-EC-EARTH shows the negative signal with decrease of discharge values by 3.1 cubic meter per second. For RCP 8.5, it ranges from 8.8 cubic meter per second to 44.8 cubic per second.

Frequency analysis of extreme low flows indicate towards increase in occurrence of low flows between 2 -9 cubic meter per second for both RCPs. Similarly, frequency of daily stream flow discharge of extreme high flows remarkable increase in number of occurrence for discharge values greater than 990 cubic meter per second, which is higher for RCP 8.5 compared to RCP 4.5.

7. REFERENCES

Abdo, K. S., Fiseha, B. M., Rientjes, T. H. M., Gieske, A. S. M., & Haile, A. T. (2009). Assessment of climate change impacts on the hydrology of Gilgel Abay catchment in Lake Tana basin, Ethiopia. *Hydrological Processes*, *23*(26), 3661–3669. https://doi.org/10.1002/hyp.7363

Abebe, N. A., Ogden, F. L., & Pradhan, N. R. (2010). Sensitivity and uncertainty analysis of the conceptual HBV rainfall-runoff model: Implications for parameter estimation. *Journal of Hydrology*, *389*(3–4), 301–310. https://doi.org/10.1016/j.jhydrol.2010.06.007

Alemseged, T. H., & Tom, R. (2015). Evaluation of regional climate model simulations of rainfall over the Upper Blue Nile basin. *Atmospheric Research*, *161–162*, 57–64. https://doi.org/10.1016/j.atmosres.2015.03.013

Amengual, A., Homar, V., Romero, R., Alonso, S., & Ramis, C. (2012). Projections of the climate potential for tourism at local scales: Application to Platja de Palma, Spain. *International Journal of Climatology*, *32*(14), 2095–2107. https://doi.org/10.1002/joc.2420

Andermann, C., Bonnet, S., & Gloaguen, R. (2011). Evaluation of precipitation data sets along the Himalayan front. *Geochemistry, Geophysics, Geosystems*, *12*(7). https://doi.org/10.1029/2011GC003513

Arnell, N. W. (1992). Factors controlling the effects of climate change on river flow regimes in a humid temperate environment. *Journal of Hydrology*, *132*(1–4), 321–342. https://doi.org/10.1016/0022-1694(92)90184-W

Bae, D. H., Jung, I. W., & Lettenmaier, D. P. (2011). Hydrologic uncertainties in climate change from IPCC AR4 GCM simulations of the Chungju Basin, Korea. *Journal of Hydrology*, *401*(1–2), 90–105. https://doi.org/10.1016/j.jhydrol.2011.02.012

Baguis, P., Roulin, E., Willems, P., & Ntegeka, V. (2010). Climate change and hydrological extremes in Belgian catchments. *Hydrology and Earth System Sciences Discussions*, *7*(4), 5033–5078. https://doi.org/10.5194/hessd-7-5033-2010

Basin, P. L., Tian, P., Zhao, G., Li, J., & Tian, K. (2011). Extreme value analysis of streamflow time series in. *Water Science and Engineering*, *4*(2), 121–132. https://doi.org/10.3882/j.issn.1674-2370.2011.02.001

Bastola, S., Murphy, C., & Sweeney, J. (2011). The role of hydrological modelling uncertainties in climate change impact assessments of Irish river catchments. *Advances in Water Resources*, *34*(5), 562–576. https://doi.org/10.1016/j.advwatres.2011.01.008

Bates, B. C., Kundzewicz, Z. W., Wu, S., & Palutikof, J. P. (2008). *Climate Change and Water*. *Climate change and water*. https://doi.org/10.1016/j.jmb.2010.08.039

Biemans, H., Speelman, L. H., Ludwig, F., Moors, E. J., Wiltshire, A. J., Kumar, P., … Kabat, P. (2013). Future water resources for food production in five South Asian river basins and potential for adaptation - A modeling study. *Science of the Total Environment*, *468–469*, S117–S131. https://doi.org/10.1016/j.scitotenv.2013.05.092

Boberg, F., & Christensen, J. H. (2012). Overestimation of Mediterranean summer temperature projections due to model deficiencies. *Nature Climate Change*, *2*(6), 433–436. https://doi.org/10.1038/nclimate1454

Chalise, S. R., & Khanal, N. R. (2001). Rainfall and related natural disasters in Nepal. In: Landslide Hazard Mitigation in the Hindu Kush-Himalayas. ICIMOD, Kathmandu, Nepal.

Retrieved from http://lib.icimod.org/record/21557/files/c_attachment_96_779.pdf

Charles, S. P., Chiew, F. H., & Zheng, H. (2016). Climate change and water in south Asia - overview and literature review.

Cruff, R. W., & Thompson, T. H. (1967). A Comparison of Methods of Estimating Potential Evapotranspiration Frcom Climatological Data in Arid and Subhumid Environments. *Geological Survey Water-Supply Paper 1839-M, United States Government Printing Office Washington*.

Dams, J., Nossent, J., Senbeta, T. B., Willems, P., & Batelaan, O. (2015). Multi-model approach to assess the impact of climate change on runoff. *Journal of Hydrology*, *529*, 1601–1616. https://doi.org/10.1016/j.jhydrol.2015.08.023

Dosio, A. (2016). Projections of climate change indices of temperature and precipitation from an ensemble of bias-adjusted high-resolution EURO-CORDEX regional climate models. *Journal of Geophysical Research: Atmospheres*. https://doi.org/10.1002/2015JD024411

E. Sanchez, R. Romera, M. A. Gaertner, C. G. and M. C. (2009). Development of a high resolution daily gridded temperature data set (1969 – 2005) for the Indian region. *Atmospheric Science Letters*, *10*(October), 249–254. https://doi.org/10.1002/asl

Feser, F., Rockel, B., von Storch, H., Winterfeldt, J., & Zahn, M. (2011). Regional Climate Models Add Value to Global Model Data: A Review and Selected Examples. *Bulletin of the American Meteorological Society*, *92*(9), 1181–1192. https://doi.org/10.1175/2011BAMS3061.1

Finger, D., Heinrich, G., Gobiet, A., & Bauder, A. (2012). Projections of future water resources and their uncertainty in a glacierized catchment in the Swiss Alps and the subsequent effects on hydropower production during the 21st century. *Water Resources Research*, *48*(2), 1–20. https://doi.org/10.1029/2011WR010733

Flato, G., Marotzke, J., Abiodun, B., Braconnot, P., Chou, S. C., Collins, W., … Rummukainen, M. (2013). Evaluation of Climate Models. *Climate Change 2013: The Physical Science Basis. Contribution of Working Group I to the Fifth Assessment Report of the Intergovernmental Panel on Climate Change*, 741–866. https://doi.org/10.1017/CBO9781107415324

Fowler, H. J., Blenkinsop, S., & Tebaldi, C. (2007). Linking climate change modelling to impacts studies: Recent advances in downscaling techniques for hydrological modelling. *International Journal of Climatology*. https://doi.org/10.1002/joc.1556

Gautam, D. K., & Phaiju, A. G. (2013). Community Based Approach to Flood Early Warning in West Rapti River Basin of Nepal. *IDRiM*, *3*(1). https://doi.org/10.5595/idrim.2013.0060

Ghimire, S., Choudhary, A., & Dimri, A. P. (2015). Assessment of the performance of CORDEX- South Asia experiments for monsoonal precipitation over the Himalayan region during present climate: part I. *Climate Dynamics*, 1–24. https://doi.org/10.1007/s00382-015-2747-2

Gleick, P. H. (1986). Methods for evaluating the regional hydrologic impacts of global climatic changes. *Journal of Hydrology*, *88*(1–2), 97–116. https://doi.org/10.1016/0022-1694(86)90199-X

Gohar, A. A., & Cashman, A. (2016). A methodology to assess the impact of climate variability and change on water resources, food security and economic welfare. *Agricultural Systems*, *147*, 51–64. https://doi.org/10.1016/j.agsy.2016.05.008

Gu, H., Yu, Z., Wang, G., Wang, J., Ju, Q., Yang, C., & Fan, C. (2014). Impact of climate change on hydrological extremes in the Yangtze River Basin, China. *Stochastic Environmental Research*

and Risk Assessment, *29*(3), 693–707. https://doi.org/10.1007/s00477-014-0957-5

Hingray, B., Mezghani, a., & Buishand, T. a. (2008). Corrigendum to "Development of probability distributions for regional climate change from uncertain global mean warming and an uncertain scaling relationship" published in Hydrol. Earth Syst. Sci., 11, 1097–1114, 2007. *Hydrology and Earth System Sciences*, *12*(1), 75–75. https://doi.org/10.5194/hess-12-75-2008

Hubert, M., & Vandervieren, E. (2008). An adjusted boxplot for skewed distributions. *Computational Statistics and Data Analysis*, *52*(12), 5186–5201. https://doi.org/10.1016/j.csda.2007.11.008

Hunt, B. G. (2007). Climatic outliers. *International Journal of Climatology*, *4*(December 2007), 139–156. https://doi.org/10.1002/joc.1379

Jiang, T., Chen, Y. D., Xu, C. yu, Chen, X., Chen, X., & Singh, V. P. (2007). Comparison of hydrological impacts of climate change simulated by six hydrological models in the Dongjiang Basin, South China. *Journal of Hydrology*, *336*(3–4), 316–333. https://doi.org/10.1016/j.jhydrol.2007.01.010

Kour, R., Patel, N., & Krishna, A. P. (2016). Climate and hydrological models to assess the impact of climate change on hydrological regime: a review. *Arabian Journal of Geosciences*, *9*(9). https://doi.org/10.1007/s12517-016-2561-0

Krause, P., & Boyle, D. P. (2005). Advances in Geosciences Comparison of different efficiency criteria for hydrological model assessment. *Advances In Geosciences*, *5*(89), 89–97. https://doi.org/10.5194/adgeo-5-89-2005

Liu, Y. B., & Smedt, F. De. (2004). WetSpa Extension , A GIS-based Hydrologic Model for Flood Prediction and Watershed Management Documentation and User Manual. *Management*, (March), 1–126.

Lu, J. biao, Sun, G., McNulty, S. G., & Arnatya, D. M. (2005). A Comparision of Six Potential Evapotranspiration Methods For Regional Use In The Southeastern United States. *JOURNAL OF THE AMERICAN WATER RESOURCES ASSOCIATION*. Retrieved from https://www.srs.fs.usda.gov/pubs/ja/ja_lu004.pdf

Lutz, A. F., ter Maat, H. W., Biemans, H., Shrestha, A. B., Wester, P., & Immerzeel, W. W. (2016). Selecting representative climate models for climate change impact studies: An advanced envelope-based selection approach. *International Journal of Climatology*. https://doi.org/10.1002/joc.4608

Minville, M., & Leconte, R. (2008). Uncertainty of the impact of climate change on the hydrology of a nordic watershed, 70–83. https://doi.org/10.1016/j.jhydrol.2008.05.033

Mishra, V. (2015). Climatic uncertainty in Himalayan water towerss. *Journal of Geophysical Research: Atmospheres RESEARCH*, 1–17. https://doi.org/10.1002/2014JD022650.Received

Moetasim Ashfaq, Ying Shi, Wen-wen Tung, Robert J. Trapp, Xueijie Gao, Jeremy S. Pal, and N. S. D. (2009). Suppression of south Asian summer monsoon precipitation in the 21st century. *Geophysical Research Letters*, *36*. https://doi.org/10.1029/2008GL036500, 2009

Nash, J. E., & Sutcliffe, J. V. (1970). River Flow Forecasting Through Conceptual Models Part I-a Discussion of Principles*. *Journal of Hydrology*, *10*, 282–290. https://doi.org/10.1016/0022-1694(70)90255-6

Nepal, S. (2012). Evaluating Upstream-Downstream Linkages of Hydrological Dynamics in the

Himalayan Region submitted to the Faculty of Chemical and Earth Sciences of the. *2012*, (May), 262.

Nigatu, Z. M. (2013). Hydrological Impacts of Climate Change On Lake Tana â€™ s Water Balance Hydrological Impacts of Climate Change On Lake Tana â€™ s Water Balance, (March), 57. Retrieved from http://www.itc.nl/library/papers_2013/msc/wrem/mulushewanigatu.pdf

Paeth, H., & Mannig, B. (2012). On the added value of regional climate modeling in climate change assessment. *Climate Dynamics*, *41*(3–4), 1057–1066. https://doi.org/10.1007/s00382-012-1517-7

Pechlivanidis, I. G., Jackson, B. M., Mcintyre, N. R., & Wheater, H. S. (2011). Catchment Scale Hydrological Modelling : a Review of Model Types , Calibration Approaches and Uncertainty Analysis Methods in the Context of Recent Developments in Technology and. *Global NEST*, *13*(3), 193–214.

PERERA, E. D. P., HIROE, A., FUKAMI, K., UENOYAMA, T., & TANAKA, S. (2013). Climate Change Impact Study on Flood Risk in Lower West Rapti River Basin Using Mri-Agcm Outputs. *Journal of Japan Society of Civil Engineers*, *69*, *No. 4*, 451–456.

Perera, E. D. P., Hiroe, A., Shrestha, D., Fukami, K., Basnyat, D. B., Gautam, S., … Tanaka, S. (2014). Community-based flood damage assessment approach for lower West Rapti River basin in Nepal under the impact of climate change. *Natural Hazards*, *75*(1), 669–699. https://doi.org/10.1007/s11069-014-1339-5

Perkins, S. E., Pitman, A. J., Holbrook, N. J., & McAneney, J. (2007). Evaluation of the AR4 climate models' simulated daily maximum temperature, minimum temperature, and precipitation over Australia using probability density functions. *Journal of Climate*, *20*(17), 4356–4376. https://doi.org/10.1175/JCLI4253.1

Pierce, D. W., Barnett, T. P., Santer, B. D., & Gleckler, P. J. (2009). Selecting global climate models for regional climate change studies. *Proceedings of the National Academy of Sciences*, *106*(21), 8441–8446. https://doi.org/10.1073/pnas.0900094106

Rajbhandari, R., Shrestha, A. B., Kulkarni, A., Patwardhan, S. K., & Bajracharya, S. R. (2014). Projected changes in climate over the Indus river basin using a high resolution regional climate model (PRECIS). *Climate Dynamics*, *44*(1–2), 339–357. https://doi.org/10.1007/s00382-014-2183-8

Rajbhandari, R., Shrestha, A. B., Nepal, S., & Wahid, S. (2016). Projection of Future Climate over the Koshi River Basin Based on CMIP5 GCMs. *Atmospheric and Climate Sciences*, *6*(2), 190–204. https://doi.org/10.4236/acs.2016.62017

Randall, D. A., Wood, R. A., Bony, S., Colman, R., Fichefet, T., Fyve, J., … Taylor, K. E. (2007). Climate Models and Their Evaluation. *Climate Change 2007: The Physical Science Basis. Contribution of Working Group I to the Fourth Assessment Report of the Intergovernmental Panel on Climate Change*, 591–662. https://doi.org/10.1016/j.cub.2007.06.045

Rao, L. Y., Sun, G., Ford, C. R., & Vose, J. M. (2011). Modeling potential evapotranspiration of two forested watersheds in the southern Appalachians. *Research & Development Treesearch*, *54*(6), 2067–2078. https://doi.org/10.13031/2013.40666

Rientjes, T. (2015). Hydrologic modelling for Intergated Water Resource. *Lecture Notes for Module 9-10 Surface Water Stream*.

Samuelsson, P., Jones, C. G., Willén, U., Ullerstig, A., Gollvik, S., Hansson, U., … Wyser, K. (2011). The Rossby Centre Regional Climate model RCA3: Model description and performance. *Tellus, Series A: Dynamic Meteorology and Oceanography*, *63*(1), 4–23. https://doi.org/10.1111/j.1600-0870.2010.00478.x

Sanap, S. D., Pandithurai, G., & Manoj, M. G. (2015). On the response of Indian summer monsoon to aerosol forcing in CMIP5 model simulations. *Climate Dynamics*, *45*(9–10), 2949–2961. https://doi.org/10.1007/s00382-015-2516-2

Seibert, J. (2000). Multi-criteria calibration of a conceptual runoff model using a genetic algorithm. *Hydrology and Earth System Sciences*, *4*(2), 215–224. https://doi.org/10.5194/hess-4-215-2000

Seibert, J., & Vis, M. J. P. (2012). Teaching hydrological modeling with a user-friendly catchment-runoff-model software package. *Hydrology and Earth System Sciences*, *16*(9), 3315–3325. https://doi.org/10.5194/hess-16-3315-2012

Syed, F. S., Iqbal, W., Syed, A. A. B., & Rasul, G. (2014). Uncertainties in the regional climate models simulations of South-Asian summer monsoon and climate change. *Climate Dynamics*, *42*(7–8), 2079–2097. https://doi.org/10.1007/s00382-013-1963-x

Talchabhadel, R., & Sharma, R. (2014). Real Time Data Analysis of West Rapti River Basin of Nepal. *Journal of Geoscience and Environment Protection*, (December), 1–7.

Teichmann, C., Eggert, B., Elizalde, A., Haensler, A., Jacob, D., Kumar, P., … Weber, T. (2013). How does a regional climate model modify the projected climate change signal of the driving GCM: A study over different CORDEX regions using REMO. *Atmosphere*, *4*(2), 214–236. https://doi.org/10.3390/atmos4020214

Teutschbein, C., & Seibert, J. (2010). Regional Climate Models for Hydrological Impact Studies at the Catchment Scale: A Review of Recent Modeling Strategies: Regional climate models for hydrological impact studies. *Geography Compass*, *7*, 834–860. https://doi.org/10.1111/j.1749-8198.2010.00357.x

Teutschbein, C., & Seibert, J. (2012). Bias correction of regional climate model simulations for hydrological climate-change impact studies: Review and evaluation of different methods. *Journal of Hydrology*, *456–457*, 12–29. https://doi.org/10.1016/j.jhydrol.2012.05.052

van Vuuren, D. P., Edmonds, J., Kainuma, M., Riahi, K., Thomson, A., Hibbard, K., … Rose, S. K. (2011). The representative concentration pathways: An overview. *Climatic Change*, *109*(1), 5–31. https://doi.org/10.1007/s10584-011-0148-z

Wilby, R. L., Hay, L. E., Gutowski, W. J., Arritt, R. W., Takle, E. S., Pan, Z., … Clark, M. P. (2000). Hydrological repsonses to dynamically and statistically downscaled climate model output. *Geophysical Research Letters*, *27*(8), 1199. https://doi.org/10.1029/1999GL006078

Xu, C. (1999). From GCMs to river flow: a review of downscaling methods and hydrologic modelling approaches. *Progress in Physical Geography*, *23*(2), 229–249. https://doi.org/10.1191/030913399667424608

Yatagai, A., Kamiguchi, K., Arakawa, O., Hamada, A., Yasutomi, N., & Kitoh, A. (2012). Aphrodite constructing a long-term daily gridded precipitation dataset for Asia based on a dense network of rain gauges. *Bulletin of the American Meteorological Society*, *93*(9), 1401–1415. https://doi.org/10.1175/BAMS-D-11-00122.1

Zhang X and Yang F. (2004). *RClimDexUserManual*. Retrieved from

etccdi.pacificclimate.org/RClimDex/RClimDexUserManual.doc